

⑧ AFOSR TR-80-0235

③ LEVEL II

⑥ RESEARCH ON NEW APPROACHES TO OPTICAL SYSTEMS FOR INERTIAL ROTATION SENSING.

AD A 082533

⑮ for Grant No. AFOSR-76-3070

⑩ G. Pavlath H. J. Shaw M. Chodorow

Prepared for
Air Force Office of Scientific Research
Bolling Air Force Base
Washington, D.C. 20332

⑨ Final rept.
1 Oct 78-30 Sep 79

⑪ 1980

⑫ 80

for the period
1 October 1978 - 30 September 1979

⑭ 51-
G.L. Report No. 3094

⑯ 2305

⑰ B2

DTIC ELECTE
S D
MAR 27 1980
B

Edward L. Ginzton Laboratory
W. W. Hansen Laboratories of Physics
Stanford University
Stanford, California

DISTRIBUTION STATEMENT A
Approved for public release;
Distribution Unlimited

409640

JB

SECURITY CLASSIFICATION OF THIS PAGE (When Data Entered)

REPORT DOCUMENTATION PAGE		READ INSTRUCTIONS BEFORE COMPLETING FORM
1. REPORT NUMBER AFOSR-TR- 80-0285	2. GOVT ACCESSION NO.	3. RECIPIENT'S CATALOG NUMBER
4. TITLE (and Subtitle) NEW APPROACHES TO OPTICAL SYSTEMS FOR INERTIAL ROTATION SENSING	5. TYPE OF REPORT & PERIOD COVERED Final 10-1-78 through 9-30-79	
	6. PERFORMING ORG. REPORT NUMBER G.L. 3094	
7. AUTHOR(s) G. Pavlath, H. J. Shaw, and M. Chodorow	8. CONTRACT OR GRANT NUMBER(s) AFOSR-76-3070 ^{new}	
9. PERFORMING ORGANIZATION NAME AND ADDRESS Stanford University Edward L. Ginzton Laboratory / Stanford, California 94305	10. PROGRAM ELEMENT, PROJECT, TASK AREA & WORK UNIT NUMBERS 2305/B2 61102 F	
11. CONTROLLING OFFICE NAME AND ADDRESS Air Force Office of Scientific Research / NE Bolling Air Force Base Washington, D.C. 20332	12. REPORT DATE 1980	
	13. NUMBER OF PAGES 76	
14. MONITORING AGENCY NAME & ADDRESS (if different from Controlling Office)	15. SECURITY CLASS. (of this report) UNCLASSIFIED	
	15a. DECLASSIFICATION/DOWNGRADING SCHEDULE N/A	
16. DISTRIBUTION STATEMENT (of this Report) Approved for public release; distribution unlimited.		
17. DISTRIBUTION STATEMENT (of the abstract entered in Block 20, if different from Report)		
18. SUPPLEMENTARY NOTES		
19. KEY WORDS (Continue on reverse side if necessary and identify by block number)		
Inertial Rotation Sensing	Single-mode Fiber	Optical Phase Detection
Sagnac Interferometer	Optical Waveguide	
Fiber Gyro	Optical Directional Couplers	
Optical Fiber	Laser Amplifier	
20. ABSTRACT (Continue on reverse side if necessary and identify by block number)		
<p>The objective of the program is to determine the potential of new fiber optic approaches to inertial rotation sensing. The system presently under investigation is a passive recirculating Sagnac system (PRS) in which light pulses from an external laser, propagating clockwise and counterclockwise around a multiturn sensing loop of single-mode optical fiber, are repetitively recirculated around the multiturn loop a multiplicity of times to increase the sensitivity of the system to inertial rotation. It is shown experimentally that five recirculations around a loop</p>		

20. Abstract (continued)

consisting of 600 meters of single mode fiber are possible using bulk optical components of standard precision, with behavior in accordance with theory. This has potential application to small rate-gyros. Work is proceeding on an all-fiber integrated version of the PRS system, which will circumvent serious optical alignment problems encountered with bulk components, and is designed to greatly increase performance as well as reducing size, weight and cost. An optical fiber amplifier being developed under a companion program will be introduced later into this system, to compensate for fiber propagation losses, forming an active re-entrant Sagnac system (ARS), designed to permit a very large number of recirculations, forming an integrating-rate-gyro with potential for extreme sensitivity.

TABLE OF CONTENTS

	<u>Page</u>
I. INTRODUCTION	1
A. Objective	1
B. Approach	1
II. SUMMARY OF RESULTS TO DATE AND FUTURE PLANS	6
III. DESCRIPTION OF WORK DURING REPORTING PERIOD	11
A. Initial System Details	11
B. Alignment Procedures	13
1. Indirect Alignment Methods	17
2. Direct Alignment Method	19
C. Modified System for Improved Recirculation	22
D. Results Obtained with Modified System	28
E. Heterodyne Phase Detection Techniques	37
 APPENDIX A - INDIRECT, FAR WALL, SPATIAL FILTER ALIGNMENT TECHNIQUE	A.1
 APPENDIX B - INDIRECT, DOUBLE FAR WALL ALIGNMENT TECHNIQUE	B.1
 APPENDIX C - DIRECT ALIGNMENT TECHNIQUE	C.1
 APPENDIX D - ALIGNMENT OF THE FIBER OPTIC GYROSCOPE FOR RECIRCULATION	D.1
 APPENDIX E - BEAM PARAMETER TOLERANCES FOR SIMULTANEOUS COUPLING OF TWO SPATIAL BEAMS INTO ONE OPTICAL FIBER	E.1
 APPENDIX F - ACCURACIES OF VARIOUS TECHNIQUES FOR SPATIAL AND ANGULAR ALIGNMENT OF TWO SPATIAL BEAMS	F.1
 APPENDIX G - HYBRID DIRECTIONAL COUPLERS FOR USE WITH A CLOSED FIBER OPTICAL LOOP	G.1

AIR FORCE OFFICE OF SCIENTIFIC RESEARCH (AFSC)
NOTICE OF TRANSMITTAL TO DDC
This technical report has been reviewed and is
approved for public release IAW AFR 190-12 (7b).
Distribution is unlimited.
A. D. BLOSE

I. INTRODUCTION

A. Objective

The objective of the present research program is to determine the potential of new fiber optic approaches to inertial rotation sensing. This includes the development of means for extending the sensitivity and basic stability of such systems. The approach involves basic device research on these new approaches and the scope includes both theoretical analysis and experimental demonstrations. This work is aimed at establishing techniques which can improve future generations of operational rotation sensing systems. In this program we have introduced new concepts for rotation sensing devices involving the use of optical fibers to form rotation sensing loops, recirculation of optical pulses in these loops, and active operation of these loops, aimed at increasing the sensitivity, stability, and optical integration times of these devices by very large factors.

B. Approach

The approach currently being pursued under the program involves a series of experiments designed to lead to a configuration which we have termed an Active Reentrant Sagnac System (ARS). The basic theory and characteristics of the ARS system are given in previous Interim Scientific Reports,¹ and in a paper,² issued under the present grant. We will

¹Ginzton Laboratory (GL) Report No. 2816 for the period 1 June 1976 through 30 September 1977, will be referred to as Report I, and GL Report No. 2925 will be referred to as Report II, in the remainder of the present document.

²H. Arditty, H. J. Shaw, M. Chodorow, and R. Kompfner, SPIE Proceedings 157, p. 138 (August 1978).

give here only a brief summary of the principles of operation; further details will be found in the references.

In the ARS system, light from an external laser is coupled into a closed fiber optic loop, containing a large number of turns. The coupling is such as to establish light waves circulating both clockwise and counterclockwise around the loop. The light is allowed to recirculate around the complete loop a large number of times. The loop is active, containing an optical amplifier to compensate for propagation losses in the loop. The phases of the light waves are sampled and measured after each transit of the waves around the loop. To facilitate this, the output of the laser is pulsed with a pulse width somewhat less than the optical transit time once around the complete loop. This leads to a time sampled output waveform whose envelope is sinusoidal in time. Measurement of the frequency of this waveform provides a measure of the rotation rate of the system, and counting of cycles of this waveform provides a measure of the angle turned through by the system in a given time interval. Alternatively, measurement of the normalized amplitude of this waveform within the first quarter cycle can provide a measure of rotation rate. This is an essentially linear system, and as such is free of the mode locking phenomena experienced with ring laser gyros.

Referring to Fig. 1, a single pulse extracted from the laser is split into two pulses by the four-port junction, and these are introduced into the N-turn loop, one clockwise and the other counterclockwise, by the directional couplers. After they have travelled once around the N-turns of the loop, they are reintroduced into the loop for a second transit, and this process is repeated until a total of K transits have been completed.

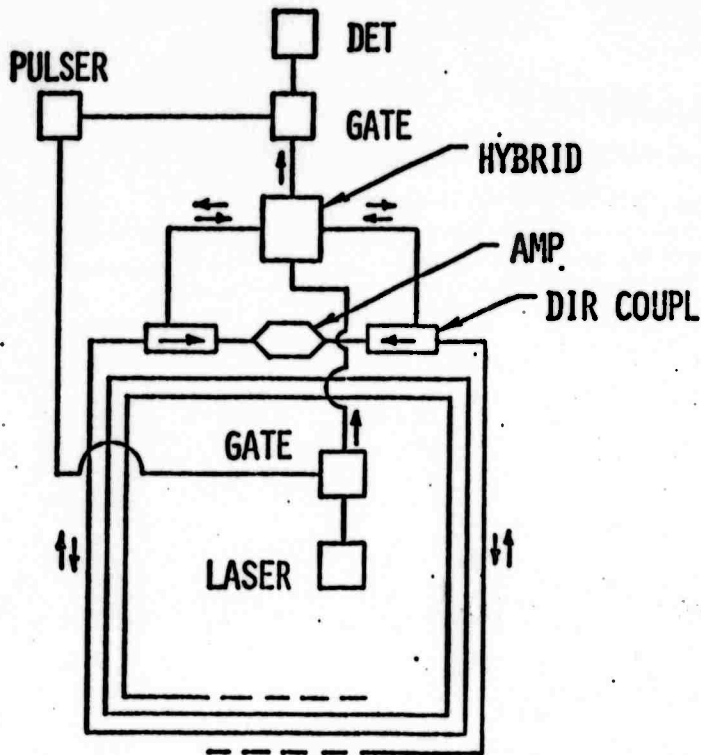


FIG. 1--ARS Schematic.

ACCESSION for	
RTS	White Section <input checked="" type="checkbox"/>
DBC	Buff Section <input type="checkbox"/>
UNANNOUNCED	<input type="checkbox"/>
JUSTIFICATION	_____
BY _____	
DISTRIBUTION/AVAILABILITY CODES	
Dist.	AVAIL and/or SPECIAL
A	

A key item is the amplifier in the loop, which compensates for propagation loss in the fiber. It is essential in order to obtain a large number of recirculations K . Increased K means increased integration time against the rotation and increased sensitivity to small rotation rates.

Each time the pulses complete a transit around the loop, they are sampled by the directional couplers. One directional coupler samples the clockwise pulse, and the other samples the counterclockwise pulse. These samples are sent back to the four-port junction, which combines them and sends them to the detector. As the original pulses continue to recirculate around the loop, they generate a train of pulse samples at the detector, as a function of time. It is important to emphasize that this entire train of output pulses results from the one single pulse extracted from the laser. The effect of rotation is to shift the phases of the optical pulses circulating around the loop. The clockwise and counterclockwise pulses are shifted in phase in opposite directions by the rotation, so that after exposure to rotation they possess a difference in phase, or relative phase shift. This relative phase shift is proportional to the rotation rate and also proportional to the length of time the pulses have been exposed to the rotation. As the pulses continue to circulate around the loop, they accumulate phase shift $\Delta\theta(t)$ which increases linearly with time t . The detector is a phase detector whose output is proportional to $\sin \Delta\theta(t)$. That is, for a fixed rotation rate, the output of the detector is a sinusoidal wave in time. An important point is that the frequency of this sinusoidal waveform is the same as the beat frequency in a standard ring laser gyro (RLG).

The present phase of work under the contract (Phase II) involves rotation sensing by passive operation of pulsed recirculating fiber optic loops, or passive reentrant Sagnac systems (PRS). This is an essential phase of the overall investigation. It is an extension of the work¹ on passive operation of cw nonrecirculating loops (Phase I), and a necessary forerunner to active operation of pulsed recirculating loops, or active reentrant Sagnac systems (ARS), which will constitute Phase III. For Phase II the system is as shown in Fig. 1, except that the amplifier is omitted.

II. SUMMARY OF RESULTS TO DATE AND FUTURE PLANS

The present project is the only known project on fiber optic gyros which is exploring the possibilities for increased sensitivity by recirculating signals repeatedly through a fiber loop. The present report covers a portion of the work under Phase II of the overall program, as described above. This portion of Phase II had the following objectives:

1. To demonstrate whether it is possible to recirculate optical pulses in single-mode fiber loops.
2. To demonstrate whether recirculated pulses increase the sensitivity to rotation in the predicted way.
3. To determine whether recirculation can be accomplished in a practical way with discrete optical bench components (lenses, prism, mirrors, etc.) used in conjunction with a single-mode fiber sensing loop.

The results of the work described in this report may be summarized as follows:

1. It was shown that optical pulses can be recirculated in a fiber optic loop.
2. It was found that recirculation increases the sensitivity of the system to rotation in the predicted way, and that the behavior is in accord with theory.
3. Using optical bench components of standard precision, it was possible to observe five recirculations of pulses in the fiber loop. This has substantial significance for fiber gyros. It multiplies the effective length of the

fiber by a factor equal to the number of recirculations. This would allow a saving in cost and size in a small gyro by reducing the total length of the fiber, allowing one to reach optimum signal-to-noise ratio with a shorter fiber. This is applicable to PRS operation as described above, where the system is operated in the recirculating mode, but passively, without an amplifier. This is of potential importance for systems operating as direct rate gyros, in ranges of relatively low rotation sensitivity, such as for guidance, and higher sensitivity, as for aircraft navigation. In such gyros, the potential interest is in a relatively small number of recirculations. Too large a number of recirculations in passive systems will result in tradeoffs and the optimum will be found in the range of small numbers.

4. The results show that optical bench components of standard precision do not have sufficient accuracy to align the system for simultaneous optimum pulse recirculation and optimum rotation sensitivity. They also lead us to conclude that more precise bulk optical components engineered for the purpose could overcome the problem. A small gyro, using a small number of passive recirculations in the passive mode (PRS mode) could be designed in this way using bulk components. It would be important to miniaturize and integrate the several elements involved into a rugged, monolithic bulk unit. We do not, however, recommend such a course, for two

reasons. First, our experience indicates that the precision and quality required in these components would be substantial, and second, a preferable, simple approach is now available, as described in paragraph 5 below.

As shown in the body of this report, the alignment problem using discrete components was investigated carefully, using a number of procedures, before arriving at the above conclusions.

5. In principle the mode and alignment problems with bulk recirculation components can be completely circumvented by use of integrated single-mode fiber components. No such components, having sufficiently high performance and low throughput loss, were available during the period that the above work was in progress. During that same period we also developed, under a companion program in the laboratory³ concerned with optical signal processing, integrated single-mode fiber optic directional couplers which appear to satisfy all requirements very well. They perform the functions of the hybrid junction and couplers of Fig. 1. The use of these integrated fiber components should eliminate all of the mode and alignment problems encountered with hybrid systems. In addition, they will provide miniaturization, ruggedness and decreased system expense. This applies to both small PRS systems with a

³Contract N00014-75-C-0632.

small number of recirculations, as discussed above, and to ARS systems with very large numbers of recirculations, forming integrating rate gyros of high sensitivity.

6. Work with the hybrid system, with final results as summarized above and given in more detail below, is completed.
7. Earlier under the present program² we introduced the principle of reciprocity in fiber gyros, and the concept that strict reciprocity will be required to avoid phase noise due to environmental effects such as temperature, vibration, etc. This requires special care in the excitation, of, and response to, the two polarization modes which exist in all fibers available in practice today. We should point out that, as described later, the PRS system is automatically reciprocal in the recirculating mode.
8. Our next immediate phase of work will involve the construction of a new integrated PRS system, with a new longer loop of lower loss fiber, and with the beam splitter and couplers of Fig. 1 being integrated single-mode fiber components. Success with the integrated components was realized shortly after the end of the present reporting period. New models will be constructed under the present program for use in the new PRS system. The work with that system will constitute the completion of Phase II.
9. Phase III of the present program will involve the addition of a fiber amplifier into the above system. An amplifier suitable

for this and other purposes is under development in another program in the laboratory.⁴

⁴Contract F33615-79-C-1789.

III. DESCRIPTION OF WORK DURING REPORTING PERIOD

A. Initial System Details

The system configuration at the beginning of the reporting period was that of a passive reentrant Sagnac interferometer (see Fig. 2) which consisted of the following components.

Laser Light Source - Initially a 5 mw HeNe laser, polarized and operating at 6328 Å .

Modulator - Coherent Associates Model 304D acousto-optic modulator, adjusted for pulse length of 1.5 μs.

Spatial Filter - Provides for control of the spatial profile of the input beam, and is also used in alignment. Initially a 15 μm pinhole was used with 45X and 10X focusing and recollimating microscope objectives.

Beam Steering Mirrors - First surface mirrors with 12% loss per reflection.

Beam Splitter - Splits the input pulse into two pulses and combines the output pulses.

Prism Directional Coupler - Closes the loop upon itself and provides for directional coupling into and out of the loop in both directions (see Appendix G for details of operation).

Fiber End Couplers - These are doublet lenses of 28.5 mm focal length which couple the spatial beams into the fiber and vice-a-versa.

Fiber Ends - The fiber ends are bonded into glass tubes. The fiber ends are then cut and polished at an angle of 26° from a plane normal to the fiber axis.

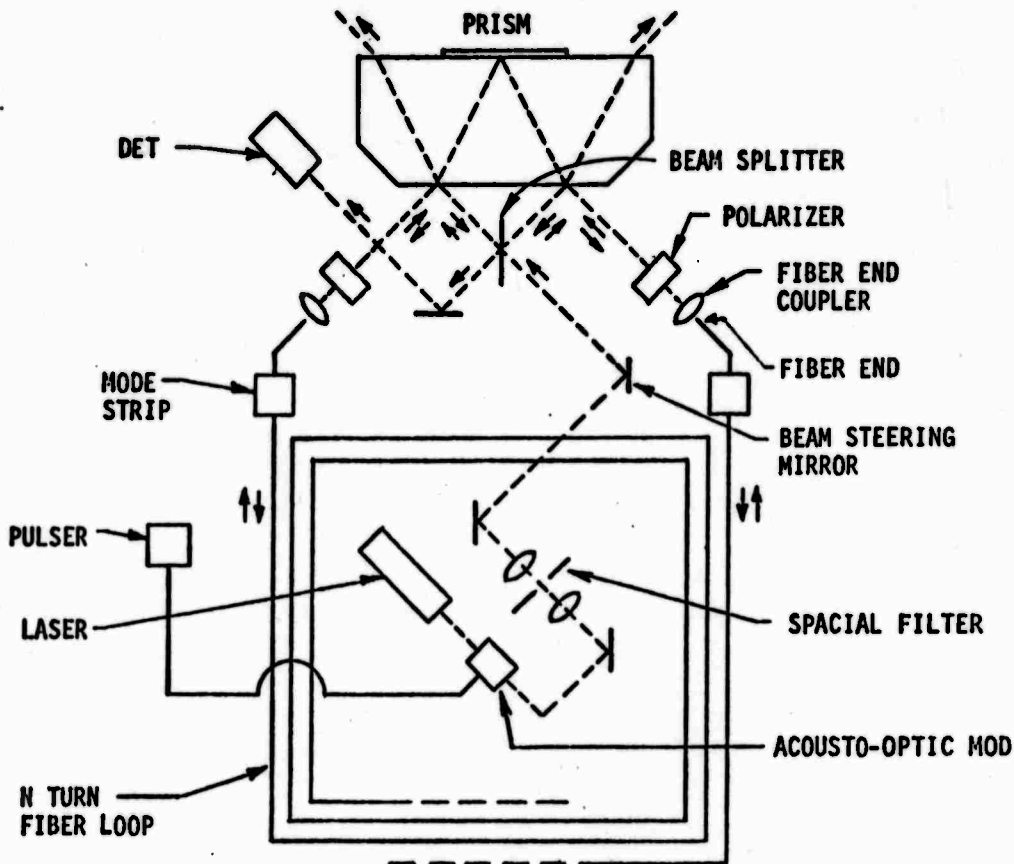


FIG. 2--Passive reentrant Sagnac inertial rotation sensor.

Fiber End Positioners - These are mechanical positioning devices which allow the fiber ends to be positioned accurately in relation to the fiber coupling lenses. Initially the fiber end positioners provided orthogonal x-y-z movement of the fiber end. The axis of the fiber was held at a fixed angle of 17° to the propagation direction of the spatial light beam. The fiber end is so positioned that the 17° and 26° angles add. The input spatial beam is incident on the face of the fiber at an angle of 43° from the normal.

The reasons for so preparing and positioning the fiber ends are as follows. First, the input light is incident on the fiber face near Brewster's angle, and hence the reflection is at a minimum for the polarization we work with. Second, the reflected spatial beam is at almost 90° to the incident spatial beam. The reflected beam leaves the system instead of being reflected back into the system where they cause rotation-insensitive spurious signals to be superimposed on the rotation-sensitive signal.

The fiber end positioners were modified with the addition of a gymbal mounting system. This gives $\pm 5^\circ$ of rotation of the fiber about a pair of mutually perpendicular axes which pass through the end of the fiber, and which are also perpendicular to the fiber axis. By having the axes pass through the fiber end, rotations about these axes are decoupled from translations in x,y, and z. The axis of the fiber is still mounted at 17° to the spatial beam. The modified fiber positioners are shown in Fig. 3.

B. Alignment Procedures

The importance of recirculating a pulse of light many times around a closed optical loop has been covered in the introduction. To demonstrate that recirculation is possible we constructed the PRS gyroscope. At the

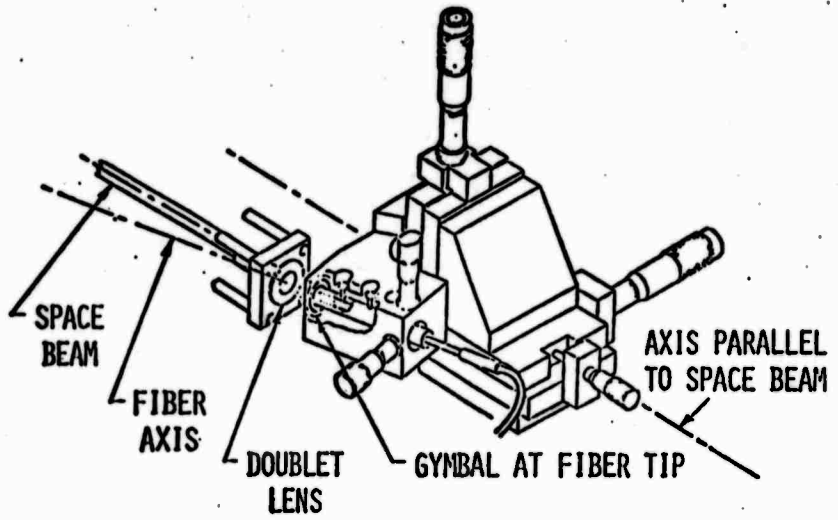


FIG. 3--Reflectionless, single-mode fiber end coupler with independent rotation and translation adjustments.

time the PRS gyroscope was constructed there were no suitable integrated optical components available. We therefore used discrete optical components which had standard tolerances and movements.

To operate a Sagnac fiber interferometer efficiently in a recirculating mode, it is necessary to solve four alignment problems, to accomplish four objectives: (1) efficient initial injection at ends of fiber loop; (2) equal initial injection at both ends of loop; (3) efficient reentry of light into fiber loop after extraction; (4) control of polarization for low noise operation (high sensitivity to rotation). Because of the small core diameter in single mode fibers (4.5μ in present case), these alignment problems present difficulties when standard types of optical bench components are used. Because the above alignment requirements are mutually interactive, straightforward cut-and-try alignment is not possible, and step-by-step protocols must be developed. This applies only to bulk systems; integrated single-mode systems will be free of this phenomenon. The alignment procedures developed under the present program are summarized below. Further details on these procedures are included in appendices.

Because of the discrete nature of the optical components the system had to be aligned to achieve efficient coupling of the clockwise (CL) propagating beams, namely the CL input and recirculating spatial beams, simultaneously into the CL fiber end. The same holds true for the counter-clockwise (CCL) propagating beams and the CCL fiber end. One wants the alignment of the CL and CCL propagating beams into their respective fiber ends to be present simultaneously, at the end of the alignment method used, in order to have satisfactory system operation, i.e., high rotation sensitivity of individual pulses and a large number of recirculations.

We have shown that it is possible to recirculate a pulse of light around a closed optical loop many times. Five recirculations of a pulse have been observed. We have also shown that recirculation behaves as predicted by theory. Because of limitations imposed by the bulk components, we were unable to align the system for simultaneous high rotation sensitivity of individual pulses and a large number of recirculations. As stated in Section II, this could be overcome through design of new, and expensive, bulk components, but in the meantime we have developed new four-port integrated fiber-to-fiber couplers³ which solve all of these problems in a simple way and offer a preferable alternative.

To align the PRS gyroscope in our investigations of recirculation we developed several alignment methods. Each successive technique was designed to overcome some deficiency which was observed in a previous technique. This section reports on the alignment methods which were tried during the reporting period. We classify them in two groups, indirect and direct.

In indirect alignment, a second laser provides an alignment beam to which the counterpropagating input beams are aligned. The fiber ends are then placed at the waist of the focused input spatial beams. If the alignment is done with sufficient accuracy, recirculation is achieved.

In direct alignment, a second laser is not used. The recirculating power is monitored directly, and adjustments are made to maximize it. When the recirculating power is maximized, the input power in both directions is maximized without disturbing the recirculating power.

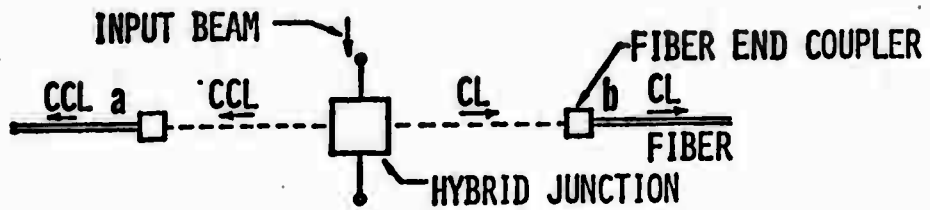
An important principle which is used in either alignment scheme is that of reciprocity. Reciprocity assures that if one of the two recirculating spatial beams couples into one fiber end with some recirculating efficiency N_R ⁵, then the other recirculating beam will couple into the other fiber end with the same efficiency N_R . Reciprocity assures us that once recirculation is achieved in one direction, it is achieved for both directions

1. Indirect Alignment Methods

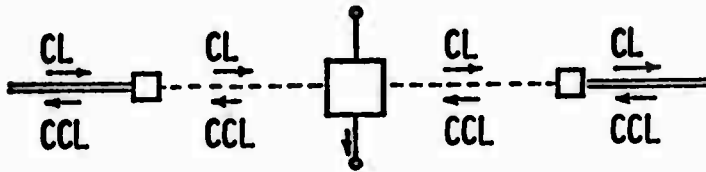
First Method

A block description of the indirect alignment procedure initially used is shown in Fig. 4. The hybrid junction consists of the beam splitter and prism coupler. Figures 4(a) and 4(b) show the spatial beam propagation for injection and recirculation, respectively. In Fig. 4(c) we see the copropagating alignment, which consists of aligning the spatial beams from the input laser and the alignment laser to be parallel and coaxial. This is achieved by causing the CCL input and alignment beams to overlap in two planes which are separated by some distance (far wall alignment). In Fig. 4(d) we see the contrapropagating alignment of the CCL alignment beam and the CL input beam. This is achieved by blocking the input beam at the source and making the necessary adjustments to cause the CCL alignment beam to propagate back through the spatial filter. See Appendix A for a detailed description of this alignment scheme.

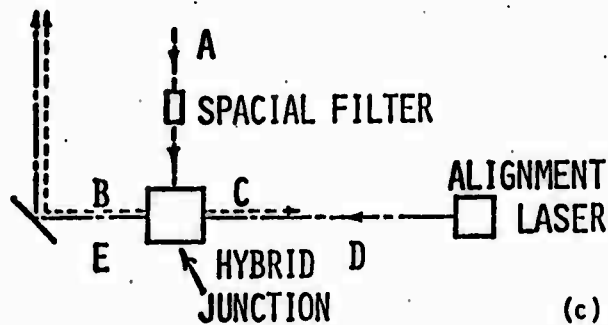
⁵The recirculating efficiency N_R is defined as the power coupled into one fiber end divided by the power out of the other fiber end.



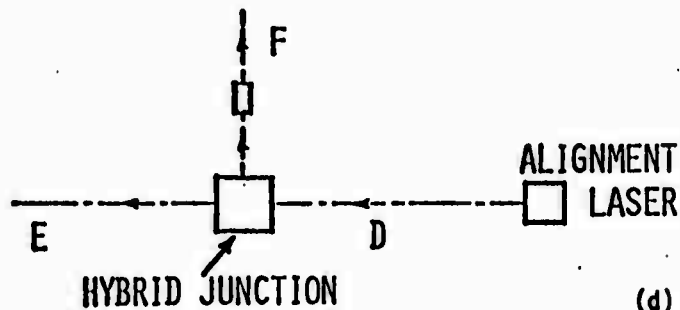
(a)



(b)



(c)



(d)

FIG. 4--Schematic of injection and recirculation alignments for initial indirect alignment technique (indirect, far wall, spatial filter alignment technique). (a) Injection. (b) Recirculation. (c) Copropagating alignment. (d) Contrapropagating alignment.

Second Method

To provide a symmetric alignment procedure we developed what we call the indirect⁶ double alignment beam-far wall alignment technique. See Appendix B for full details. In this procedure (see Fig. 5) we had alignment beams propagating in each direction. The contrapropagating alignment beams were first made to be parallel and coaxial. The contrapropagating input beams were aligned with their copropagating alignment beams using the far wall alignment technique. When the alignment is finished, the fiber ends are positioned for maximum throughput of the input beams.

2. Direct Alignment Method

The two previously stated alignment techniques were indirect. An alignment spatial beam, to which the contrapropagating input spatial beams are aligned by some method, is required. These alignment processes took about one day to perform. In order to simplify the alignment process we developed a direct alignment technique in which the recirculating power could be monitored directly.

This alignment method (see Fig. 6) uses a short piece of optical fiber which is used to simulate one end of the fiber loop as a target for the recirculating spatial beam. One end of the fiber loop is used as a source for the recirculating spatial beam. By monitoring the power out of the short fiber one can directly measure the accuracy of the recirculating alignment and monitor the effects of adjustments on the recirculating alignment in real time. Once the recirculating alignment is satisfactory,

⁶Indirect in the same sense as before.

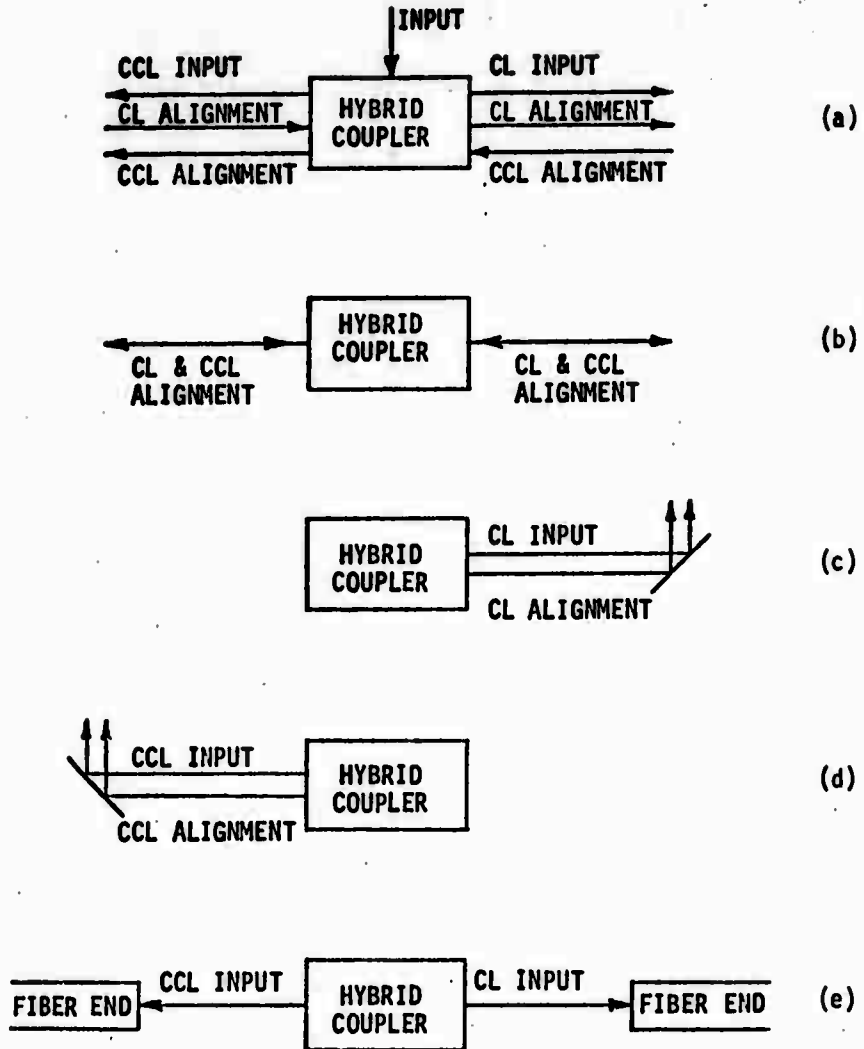


FIG. 5--Double far wall alignment procedure. (a) Beams in initial state. (b) CL and CCL alignment beams parallel and coaxial. (c) CL alignment using far wall technique. (d) CCL alignment using far wall technique. (e) Position fiber ends on input beams.

TARGET FIBER (LONG)

SOURCE FIBER (SHORT)

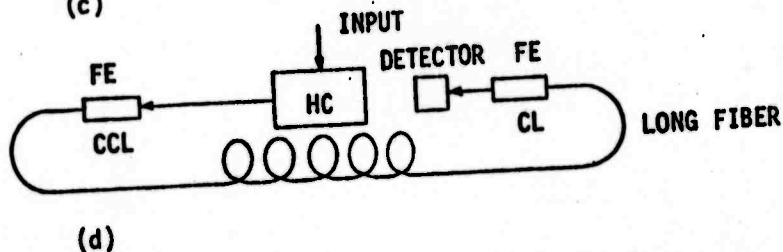
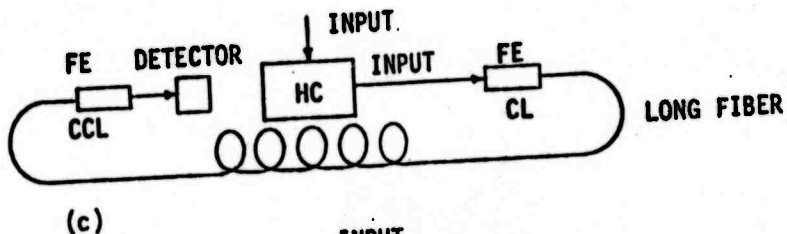
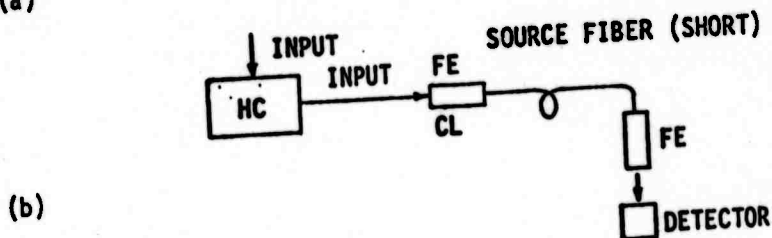
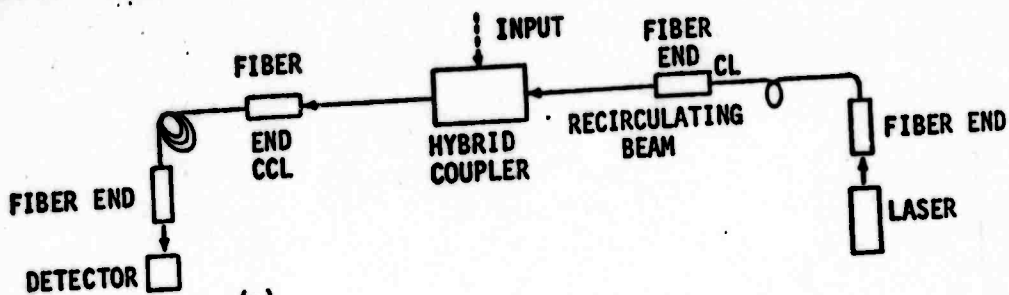


FIG. 6--Direct alignment procedure. (a) Alignment for recirculation. (b) Fix position of source fiber in space. (c) Place free end of long fiber in exact position of target fiber. (d) Couple input power into CCL fiber end.

the target fiber is removed and the free end of the fiber loop is placed in its exact position. Input power is then optimized in both directions. See Appendix C for full details.

This alignment procedure was never implemented in its entirety due to our inability to control the spatial profile of the input beams in the proper manner and to the required accuracy. We were able to partly use this procedure to obtain limited recirculation in one direction. We observed two echoes.

All of the alignment methods worked well enough to show that recirculation is possible and that it behaves according to theory. None of the alignment methods could achieve simultaneous good rotation sensitivity of individual pulses and a large number of recirculations.⁷ This was entirely due to the tolerances and quality of the discrete optical components.

C. Modified System for Improved Recirculation

The initial system configuration, using the first method of indirect-alignment produced two rotation-sensitive echoes⁸ (see Fig. 2) with the second echo being in the range of 7 to 20 dB lower than the first. The attenuation of the N-turn fiber loop was 6 dB per transit. A third echo was never observed in the initial system configuration. Calculations indicated that the third echo was below noise.

⁷ See Appendices D and E for discussion of the tolerances on the beam parameters for alignment.

⁸ The Kth echo is a pulse of light at the output port which is caused by a pulse which has transited the N-turn optical loop K times.

Attention was given to modifying the system described previously to obtain more recirculations of the pulses. Three areas were identified where improvement could be made namely reduction in noise, improvement in alignment accuracy, and higher input power.

Noise problems were brought under control by standard modifications to reduce scattered light and circumvent EMI pickup in the electronic circuits. Dark current in the PM tube, which would be a factor when studying ultimate sensitivity to small rotation, was not a factor in the present measurements. Cooling of the PM tube is available for future rotation-sensitivity measurements.

To improve the alignment accuracy of the first method of indirect alignment described previously, the spatial filter, which is a key element in the alignment process, was redesigned. The original 15 μm pinhole was replaced with a 5 μm pinhole, and required modifications were made in the pinhole carrier, recollimating lens carrier, and the focusing and recollimating microscope objectives. This brought the contrapropagating alignment accuracy equal to the copropagating alignment accuracy which initially was 2.5 times better.⁹

We found that the accuracy achieved with the recirculation prism could not be improved upon by substitution of separate components which decouple the recirculating and input beam parameters. One procedure involves the use of two optical blanks and two mirrors in place of the prism (Fig. 7). Adjustment of the optical blanks adjusts the input beam directly but affects the recirculating beam in second order only.

⁹See Appendix F for a discussion of the accuracies of the alignment techniques.

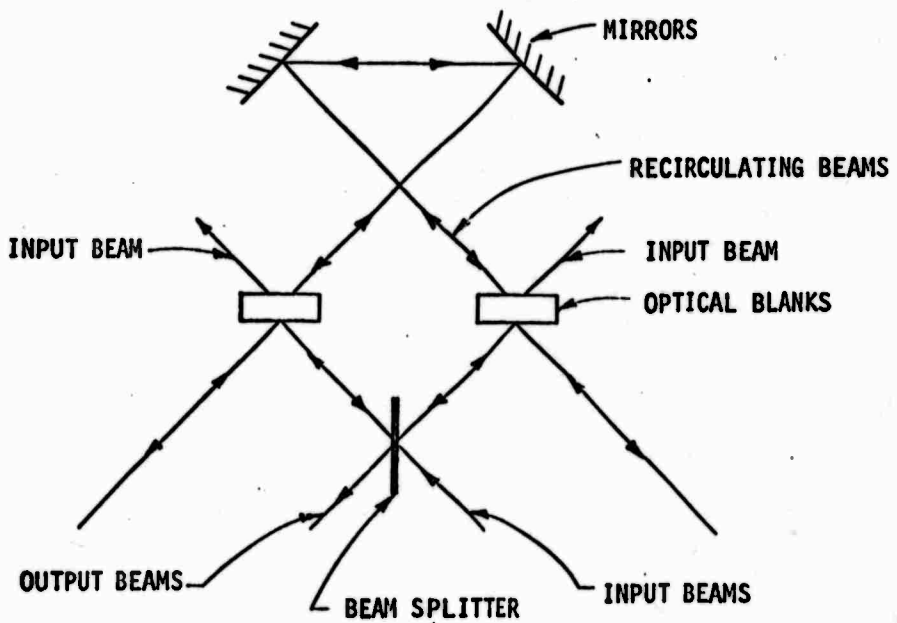
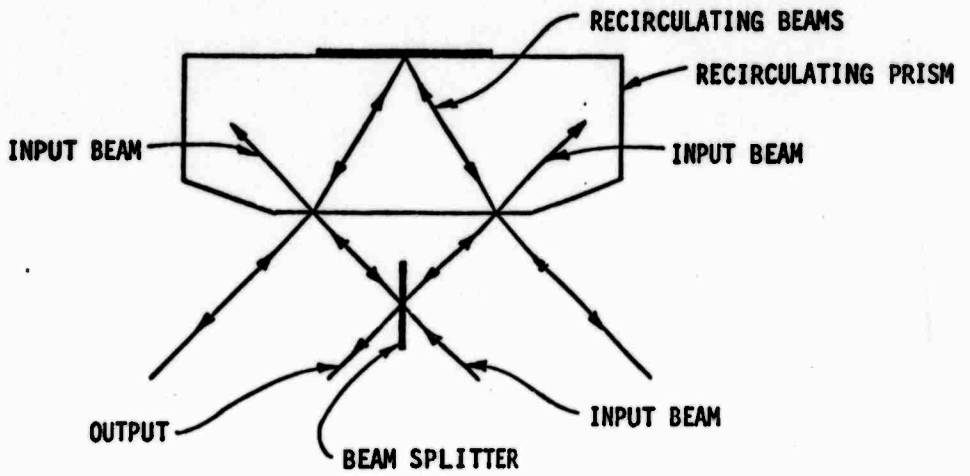


FIG. 7--Recirculating prism and replacement.

Adjustment of the two mirrors adjusts only the recirculating beam. Any lenses placed between the optical blanks will transform the recirculating beam only. This configuration proved to be impractical because of resolution and instability problems with the separate components, as compared to the integrated nature of the prism. We retained the recirculation prism for subsequent experiments.

To obtain higher input powers a Spectra-Physics model 125 He-Ne laser, without mirrors but with power supply was obtained at no cost to the contract. The necessary mounting and beam steering hardware was fabricated and the laser was installed on the rotating table. The mounting arrangement is shown in Fig. 8 and Fig. 9. The increase in effective power¹⁰ was less than expected, but was sufficient for our purposes. It increased from 4 mW with the previous laser to 17 mW with the new laser. Although the new laser is capable of 50 mW output, it was reduced by losses in a reducing telescope and additional beam steering mirrors which were required. With regard to the reducing telescope, it was necessary to construct such an instrument to match the spot size of the new laser to that required by the acousto-optic modulator. A moderately extensive physical modification of the system was also required to cope with heating problems encountered with the Model 125 laser after installation on the rotating table. The internal adaptations and output power of this laser are critically sensitive to temperature and require adequate cooling.

¹⁰Effective power is defined as the modulated power at the input to the spatial filter.

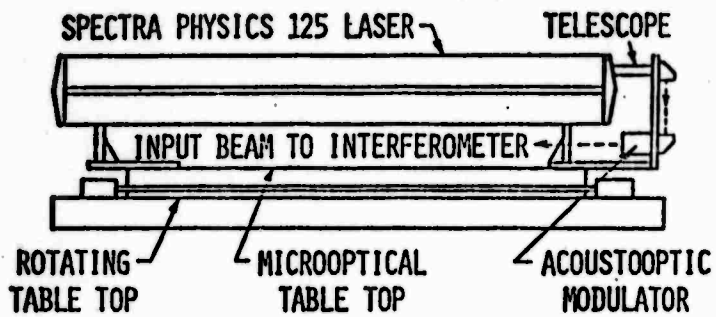


FIG. 8--Laser mounting.

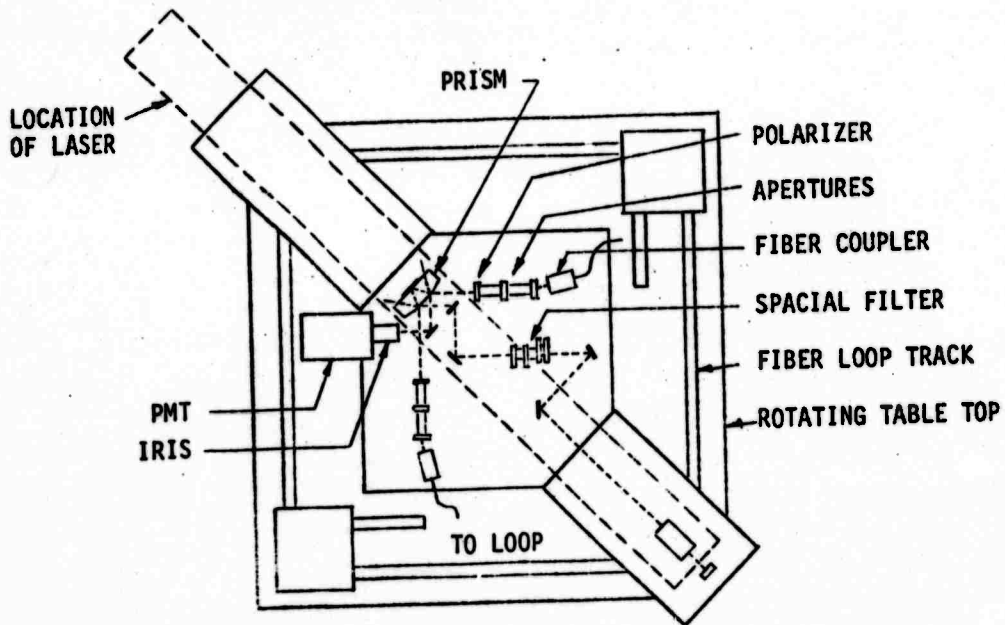
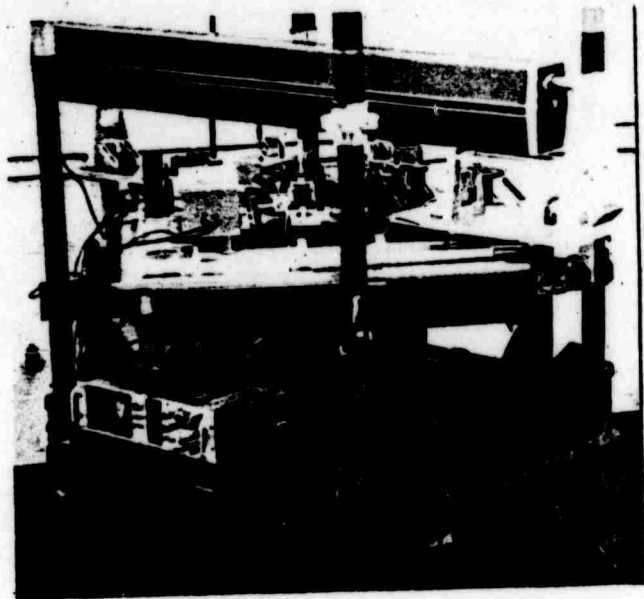


FIG. 9--Experimental system.

D. Results Obtained with Modified System

When the modified system was aligned using the first method of indirect alignment, two rotation-sensitive echoes were obtained, and this number could not be increased by formal realignment. Significantly, it was found that, by moving one of the fiber ends closer to its coupling lens the number of echoes could be increased, to a total of five echoes. Furthermore, it was found that these echoes were now only slightly rotation sensitive. This result was observed consistently. Further theoretical and experimental studies, as shown below, have led to an understanding of this result. The resulting explanation is as follows. It is found that recirculation has indeed been established with equal efficiency for both directions of circulation. However, an asymmetric input condition exists which leads to a significant level of power flow in one direction only. Furthermore, we find that this asymmetry is due to unmatched spatial profiles for the input and recirculating beams. We can thus conclude that these profiles would need to be matched if a system having both large numbers of recirculations and high rotation sensitivity per circulation, were to be designed using bulk injection and recirculation components. The studies investigating these conclusions are described below and in the appendices.

Figures 10(a) and (b) are photographs of typical oscilloscope traces which we obtained. The vertical axis is linear in power and the horizontal axis is linear in time. The vertical gain on the oscilloscope was increased five times for Fig. 10(b) over that for Fig. 10(a). Each figure contains three consecutive pulse trains. Each pulse train is the result of injecting a new input pulse into the fiber loop and tapping a fraction of the

PULSE
POWER

↑
→ TIME

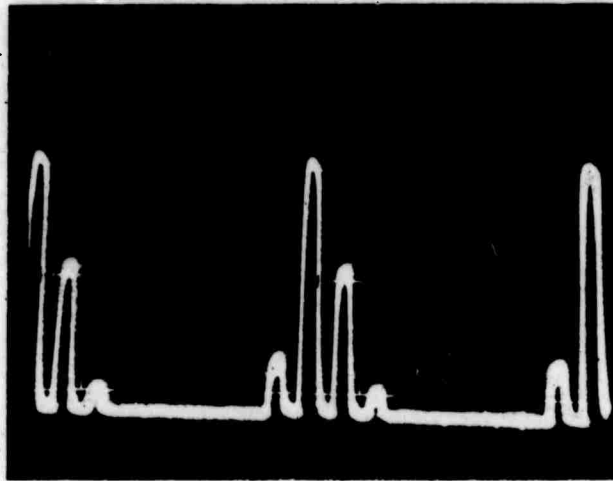


FIG. 10(a)--Oscilloscope photograph of pulse trains.

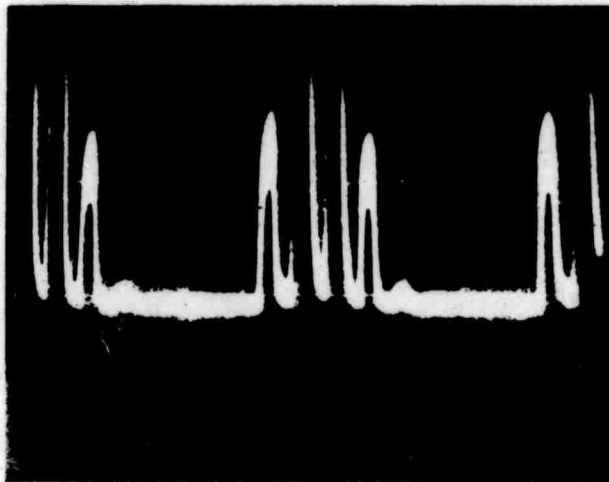


FIG. 10(b)--Oscilloscope photograph of same pulse train as above but at 5X vertical gain on the oscilloscope.

pulse power after each transit of the loop. Observe the central pulse train in each figure. The first pulse is smaller than the succeeding pulses. This first pulse is a zero order pulse. It is caused by stray light which gets to the detector without transiting the fiber optic loop. The second pulse goes through the loop once, the third pulse goes through the loop twice, etc. One expects to observe an exponential decay of the pulse amplitudes. This is not apparent in Figs. 10(a) and 10(b) due to the saturation of the detector by the first and possibly the second order echoes, while if the gain of the detector is reduced, then the third and fourth order echoes are not visible. A logarithmic amplifier was not available at the time of the measurements.

Figure 10(a) shows the first, second, and third order echoes. In Fig. 10(b), the fourth order echo is visible. These echoes are only slightly rotation sensitive, as a result of the unbalanced input signals described above.

Two potential sources for the observed asymmetric input condition can be postulated. The first is the fact that the first method of indirect alignment uses two different methods for aligning the input and recirculating beams in the CL and CCL legs. The second is that we did not attempt in any of the alignment methods, to match the spatial profiles of the input and recirculating beams. We now know that the second source is the correct one (see Appendix D for details).

To test the first postulate, that the first method of indirect alignment was the source of the asymmetric inputs, we developed the second method of indirect alignment previously, which is symmetric in the alignment of the CL and CCL legs. The same results were obtained with the second method as with the first.

To test the validity of the second postulate, concerning mode matching, we undertook a computer aided study of the propagation of Gaussian beams in a simplified version of our system. This simplified system had all the fundamentals of the complete system.

The model which was analyzed is shown in Fig. 11(a). A Gaussian beam of waist size W and radius of curvature $= \infty$ was introduced midway between the lenses. The positions of the focused waists are computed to be d_1 and d_2 . The fiber ends were positioned at the focused waists (see Fig. 11(b)). Fiber end No. 1 was assumed to radiate a Gaussian beam of waist radius equal to the radius of the core of the fiber. The radius of curvature at fiber end No. 1 was assumed to be infinite. This recirculating Gaussian beam was propagated left to right using standard formulas. The waist radius and radius of curvature of the recirculating Gaussian beam were calculated at fiber end No. 2 (see Fig. 11(c)).

Figure 12 shows the spot radius of the input beam and recirculating beam at fiber end No. 2 versus waist radius of the input beam midway between the lenses. We see that at an input beam radius of about 2.3 mm, the input and recirculating beam waist radii are equal to the core radius of the fiber. This is a good operating point. Another operating point exists at input beam radius of about 60 μm but this is not a good operating point because of the sensitivity of the operating point to misalignments.

Figure 13 shows the radius of curvature at fiber end No. 2 for the recirculating beam versus waist radius of the input beam midway between the lenses. We see that an input beam radius of 2.3 mm results in the wavefront of the recirculating beam at fiber end No. 2 being nearly planar, i.e., having a waist, as desired.

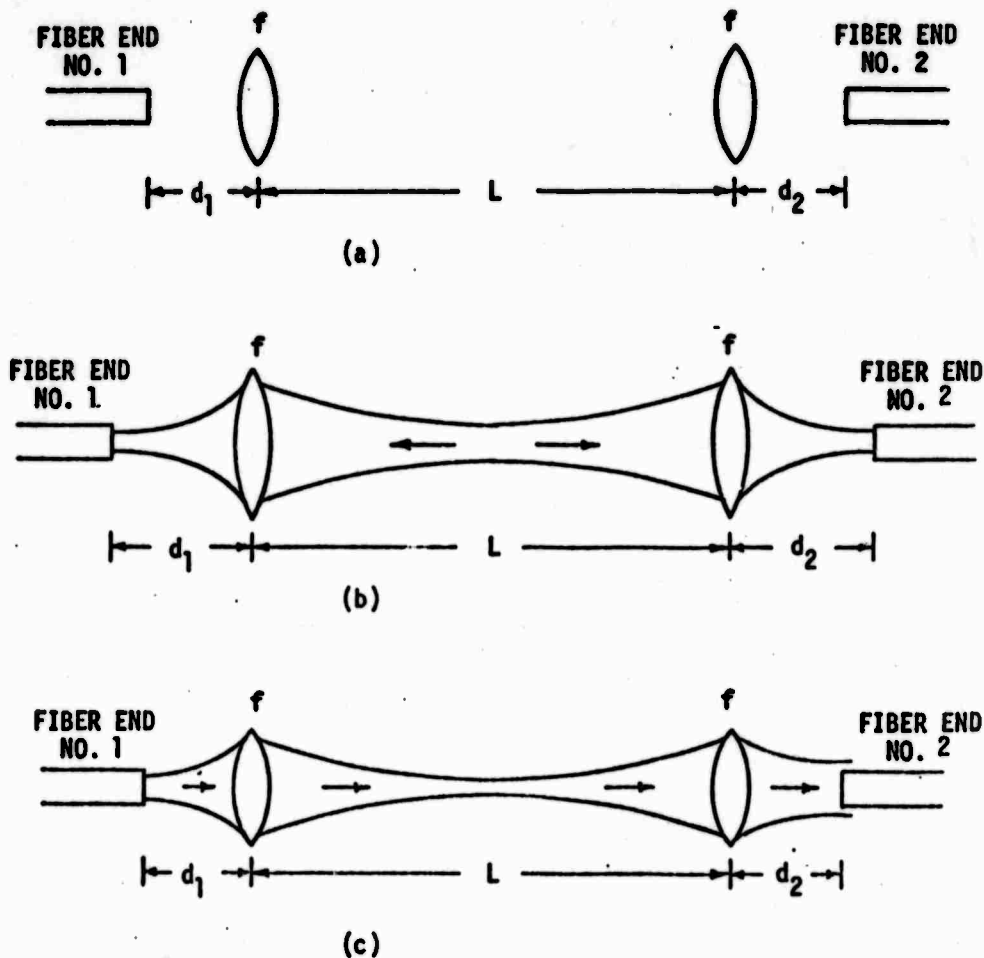


FIG. 11--System and steps in numerical analysis of mode matching of recirculating and input spatial beams. (a) System which was analyzed. (b) Contrapropagating input beams fix d_1 and d_2 . (c) Propagation of recirculating beam from left to right.

f = 25.5 mm
d = 25 cm
4.5 μ m core

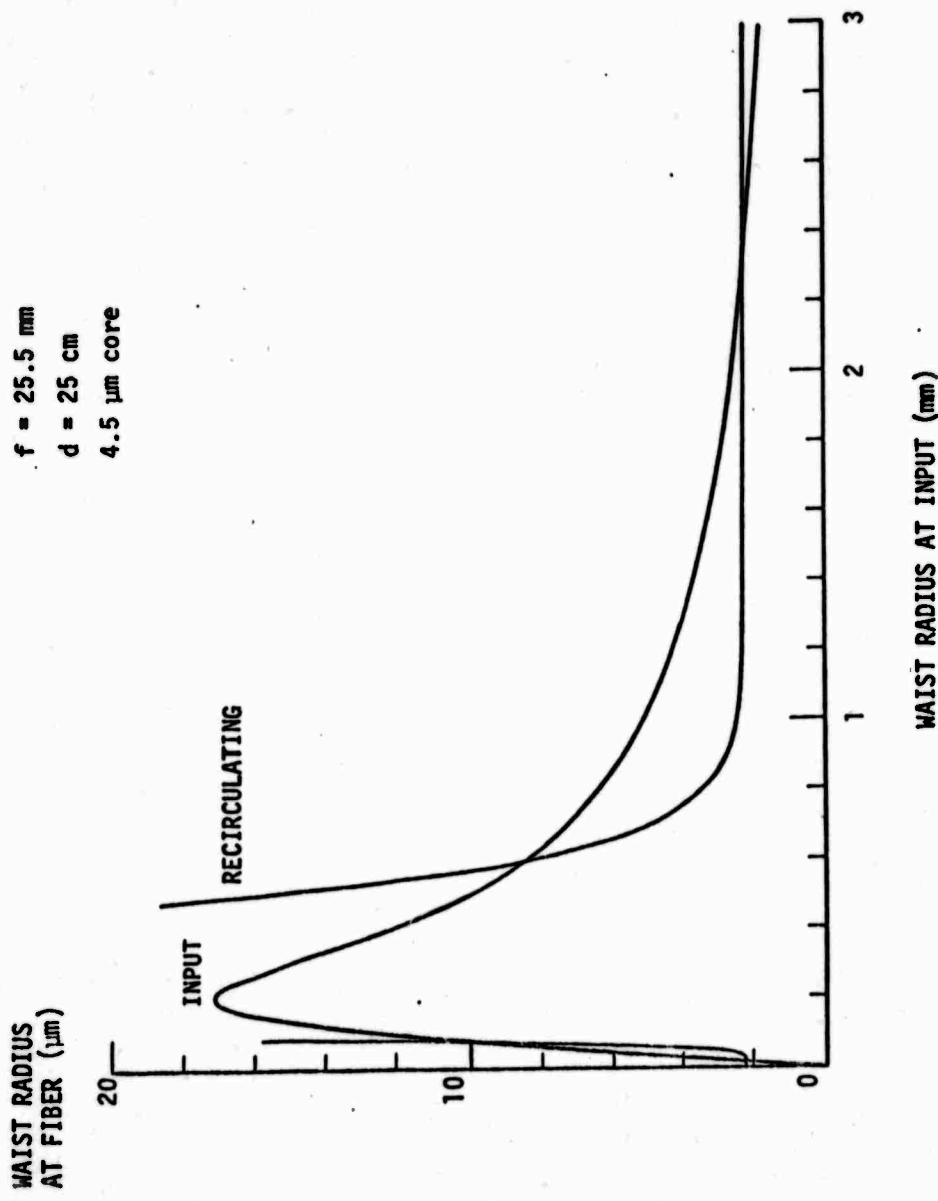


FIG. 12--Spot radius of input and recirculating beam at fiber end vs. waist radius of input beam.

RADIUS OF CURVATURE AT FIBER
OF RECIRCULATING BEAM (mm)

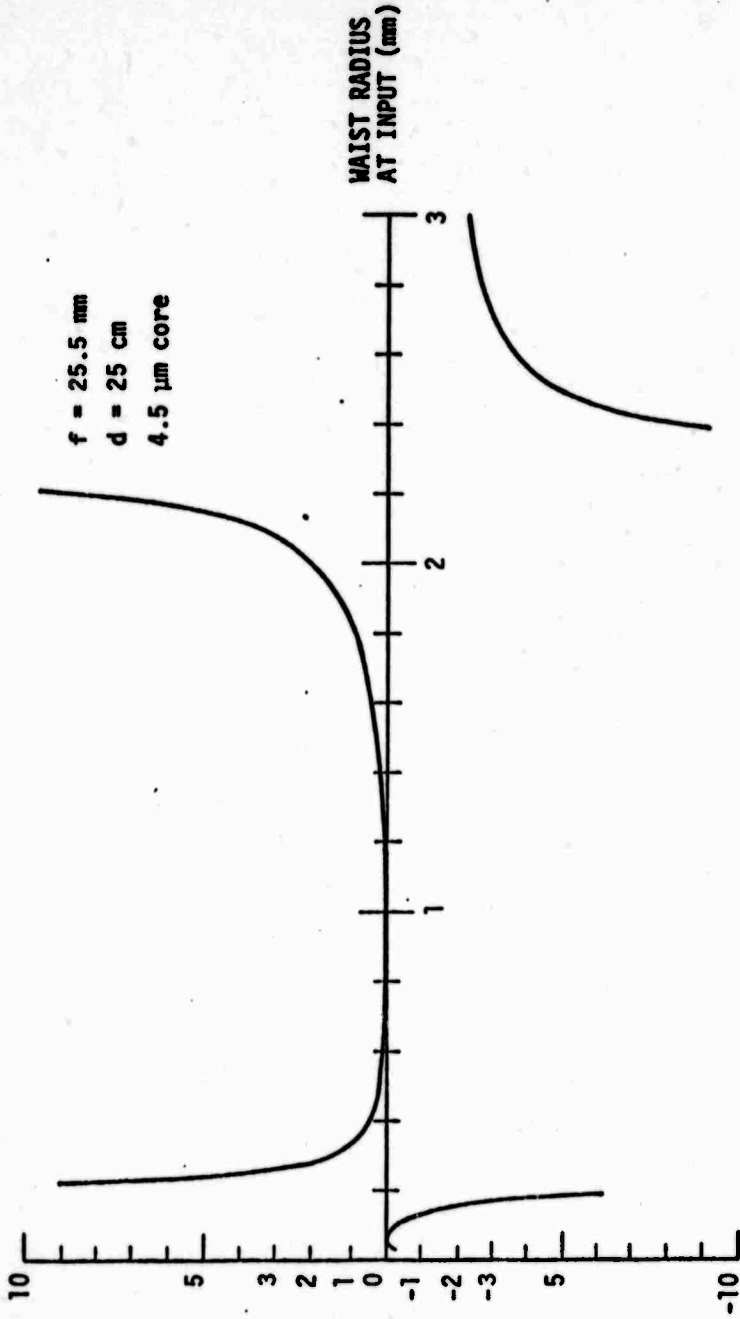


FIG. 13--Radius of curvature at fiber end
vs. waist radius of input beam.

Figure 14 shows the distance that a Gaussian beam, of radius of curvature R , is focused to by a lens of focal length 25 mm. The radius of curvature, R , is measured at the lens. This graph is accurate for values of the beam radius, r_l , measured at the lens, such that $\pi r_l / \lambda \gg f$.

This change in effective focal length¹¹ due to the radius of curvature of a Gaussian beam was observed in our previous alignment attempts. The recirculating spatial beam and the input spatial beam have different radii of curvature at the coupling lens. This results in the waists being in two different parallel planes. We can position the fiber to be in only one plane. Hence, we can have either good rotation sensitivity (balanced input power) with poor recirculation (only 2 echoes) or good recirculation (4 to 5 echoes) with low rotation sensitivity (unbalanced input power).

Mode matching in the present system would require additional lenses in the input spatial beam, and a complete redesign of the entire optical system would be required to accommodate this. In this connection, it can be observed that the procedure might, even then, not necessarily be straightforward. The problem remains that we are dealing with real lenses which have various aberrations. Assume the mode matching is accomplished to the desired degree of accuracy and that two echoes are at first observed. The next step in the alignment procedure is to adjust the appropriate controls for a maximum number of echoes. Because of the real nature of the components involved it is quite possible that the path to a global optimum for recirculation lies in a region where the second echo becomes lost in

¹¹ Effective focal length is the distance from the lens to the waist of a focused Gaussian beam.

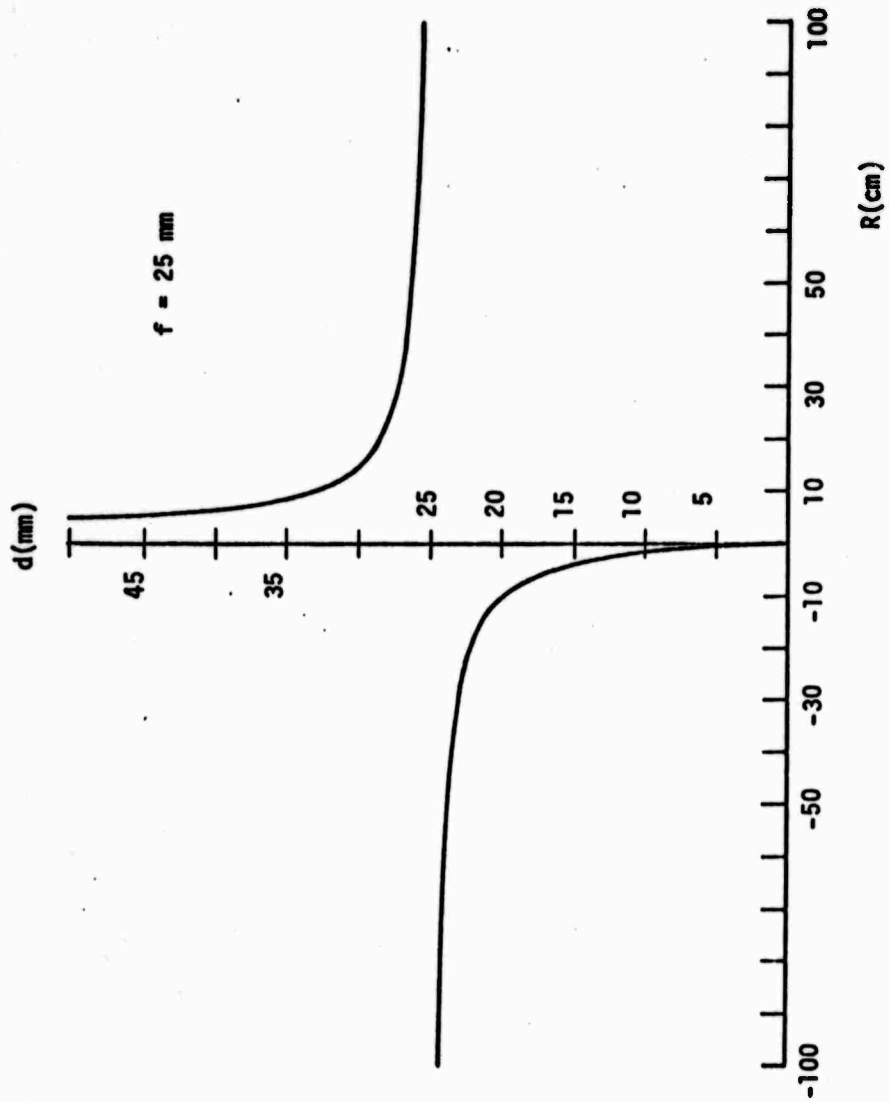


FIG. 1. Distance at which a Gaussian beam is focused by a lens vs. radius of curvature of the Gaussian beam at the lens.

the noise. We have consistently found that once the echo is lost, the system is misaligned with further adjustment. A different path to the global optimum might keep us out of this region, but such a path is not known at this time. These questions are being circumvented by the transition to integrated fiber couplers.

The fiber directional coupler program referred to above has produced a coupler for use at 1.06 μm . The coupling coefficient can be adjusted continuously from a maximum of -1 dB down to any desired value. We plan to fusion weld the ends of the fiber loop to the appropriate parts of the coupler, and will have then eliminated all problems of alignment (see Fig. 12).

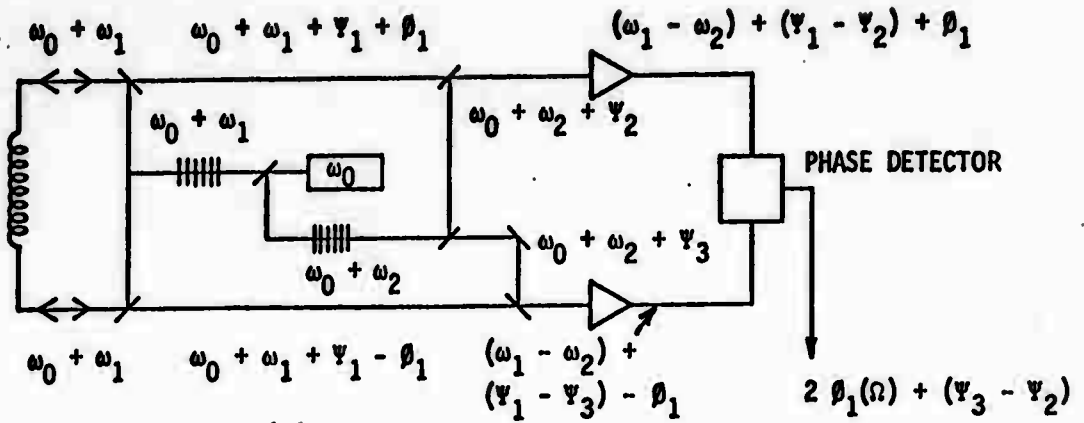
E. Heterodyne Phase Detection Techniques

As stated above, the next step will involve the construction of an integrated, all-fiber optical system. Eventually, it will be important to include solid-state sources and detectors. This requires attention to the higher noise levels in solid state detectors. We have devised a circuit designed to handle this problem without introducing phase noise in the operation of the sensing loop. The noise is inversely proportional to the frequency of the signal and, therefore, optical heterodyne detection techniques are attractive. A local oscillator is used, whose frequency is slightly shifted with respect to that of the signal to be measured. Both the signal and the local oscillator output are received simultaneously. The high optical frequencies are integrated out and only low and intermediate frequencies are detected. By the use of IF amplifiers, which filter out the dc components, one retains the high frequency component which has higher signal-to-noise ratio.

When introducing a local oscillator into the system, one should keep in mind that the coherence length of the laser source must be longer than the path difference between the signal and the local oscillator pulse. This is usually the case when a source with long coherence length (such as the He/Ne laser) is used. In integrated optics one needs a more compact source, such as an injection laser. However, its coherence length is comparatively short, thus seriously limiting us to heterodyne detection with small path differences. This implies that the local oscillator pulse must virtually be transmitted through the long fiber coil, exactly as the signal itself.

Heterodyne schemes have recently been described. In one of these,¹² shown in Fig. 15, the source is a red He/Ne laser with long coherence length. In the diagram we indicate some sources of potential noise. The main flaw is that the two legs of the local oscillator are not exactly balanced and, in fact, are embedded in slightly different environments. This in turn may give rise to uncontrolled phase difference $\psi_3 - \psi_2$, as indicated in the figure. A second case¹² is shown in Fig. 15, which uses a GaAs laser source. The coherence length is much shorter than in the previous case. Thus the local oscillator frequency $\omega_0 + \omega_2$ is transmitted through the same fiber, and in both directions, as the signal of frequency $\omega_0 + \omega_1$. Now one may have two different sources of uncontrolled phase shifts. Firstly, the two frequencies $\omega_0 + \omega_1$ and $\omega_0 + \omega_2$ may be affected in different ways by temperature fluctuations or by mechanical variations, even though both propagate along exactly the same path inside

¹² D.E. Thompson, D.B. Anderson, S.K. Yao, and B.R. Youmans, Appl. Phys. Lett. 33, 940 (1978).



LOOP MIXER (e.g. SAW ARRAY)

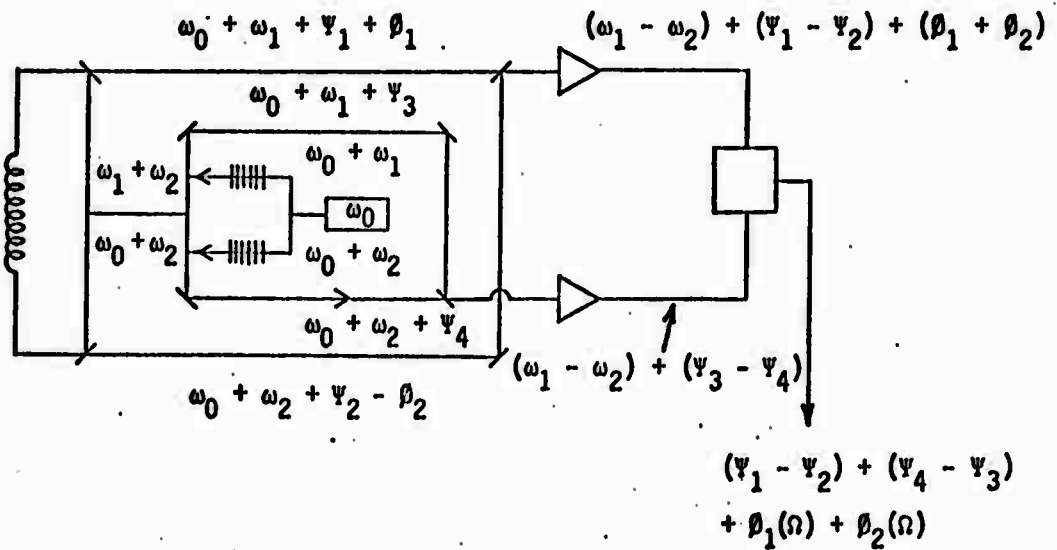


FIGURE 15

the fiber coil. Secondly, out of the fiber coil, the two frequencies propagate through different paths, causing two different phase shifts ψ_3 and ψ_4 .

We propose a simple heterodyne system (Fig. 16) which is free of the above mentioned flaws. The idea is to use one beam only, of frequency $\omega_0 + \omega_2$, that acts as a reference or carrier frequency. By mixing the beams, integrating and filtering out both the very high optical frequencies and the dc components, one obtains two signals of the same frequency $\omega_1 - \omega_2$, but different phases as shown in the figure. Utilizing a phase detector, one can easily retrieve the useful rotation sensitive phase information. Note that any optical path of the local oscillator pulse might be appropriate since its phase and frequency are eventually not taken into account. However, in case of a GaAlAs laser of short coherence length, the beam should go through the same fiber coil as the signal, in order to minimize path length differences.

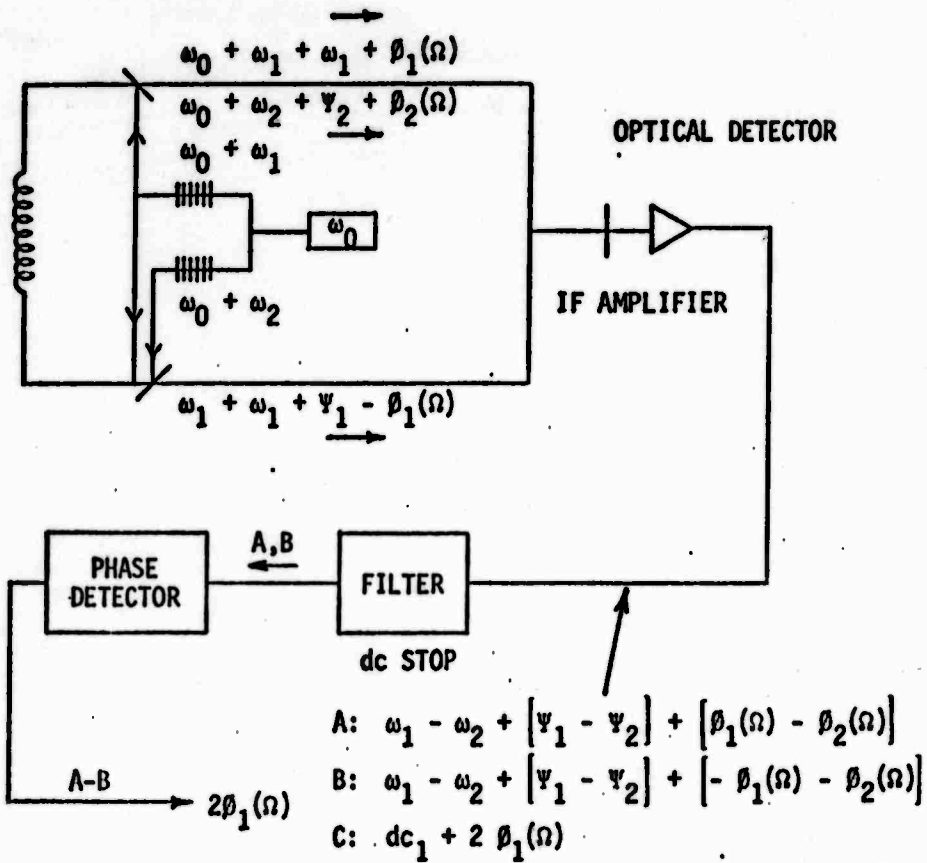


FIGURE 16

APPENDIX A

INDIRECT, FAR WALL, SPATIAL FILTER ALIGNMENT TECHNIQUE

This alignment procedure uses a second, small laser hereafter called the alignment laser to simulate the recirculating spatial beam. The two contrapropagating input spatial beams are aligned to the single alignment spatial beam using the far-wall technique for the co-propagating beams (i.e., input beam propagates in same direction as alignment beam) and the spatial filter technique for the contra-propagating beams (i.e., input beam and alignment beam propagate in opposite directions). At no time during the alignment can the recirculating efficiency be directly measured. It can only be indirectly estimated.

The following steps are what were used to align the fiber optic gyroscope using this technique in every day experiments.

- (1) Install the alignment laser and the alignment beam steering mirrors (AM3, AM2) for the alignment laser as shown in Fig. A-1.
- (2) Insert 2, 20 mil pinholes (see Fig. A-2 for diagram of a pinhole and installation of pinholes in fiber legs) in the CL fiber leg and use the alignment beam steering mirrors to send the alignment beam through the 2, 20 mil pinholes. See Fig. A-1.
- (3) Remove the pinholes in the CL fiber leg.
- (4) Install two 20 mil pinholes in CCL fiber leg and use the prism directional coupler to send the alignment beam through the two 20 mil pinholes. See Fig. A-1.

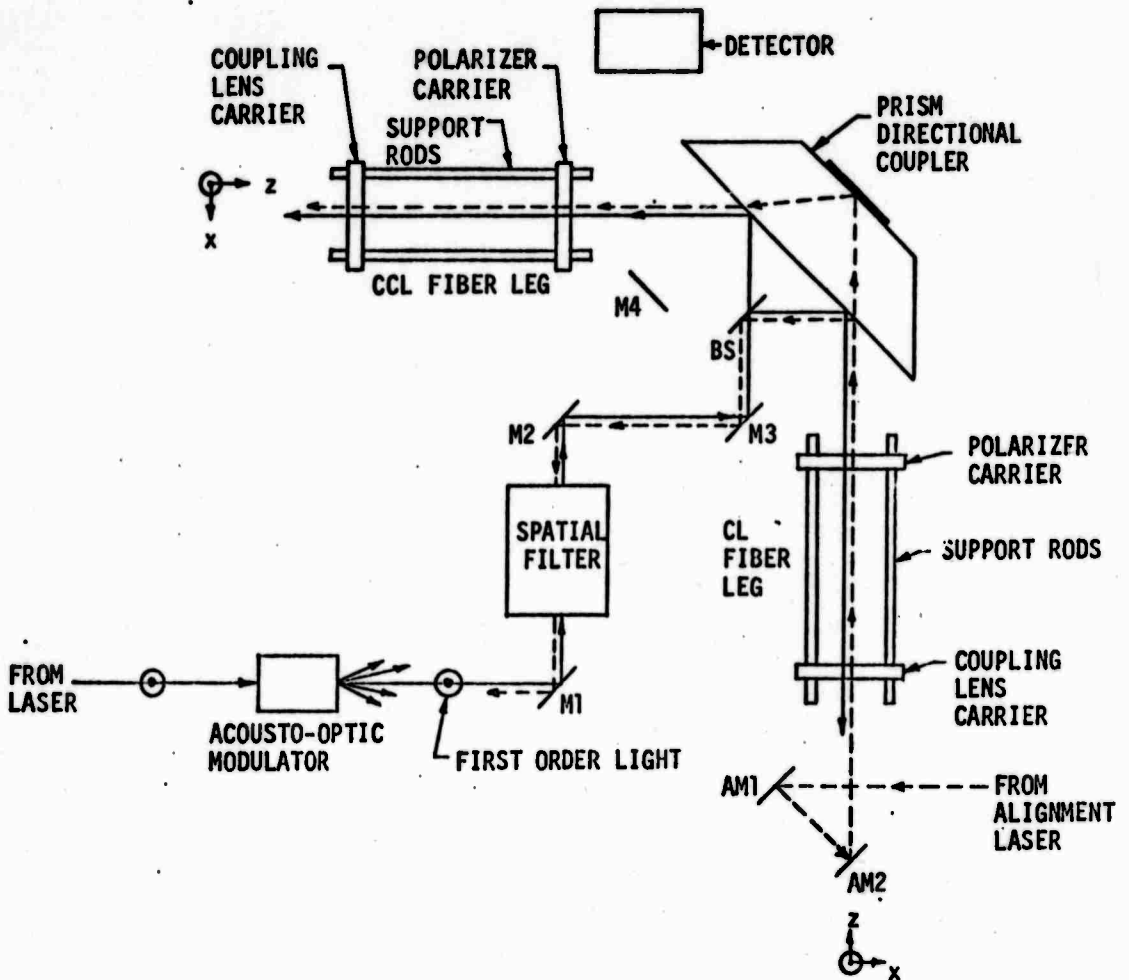
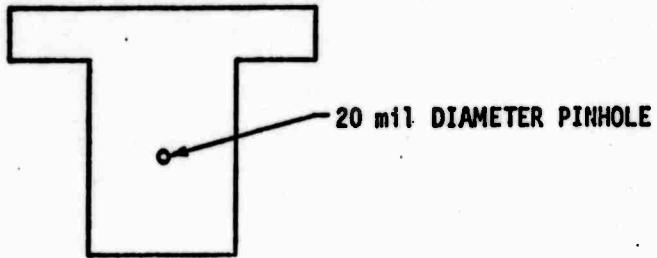
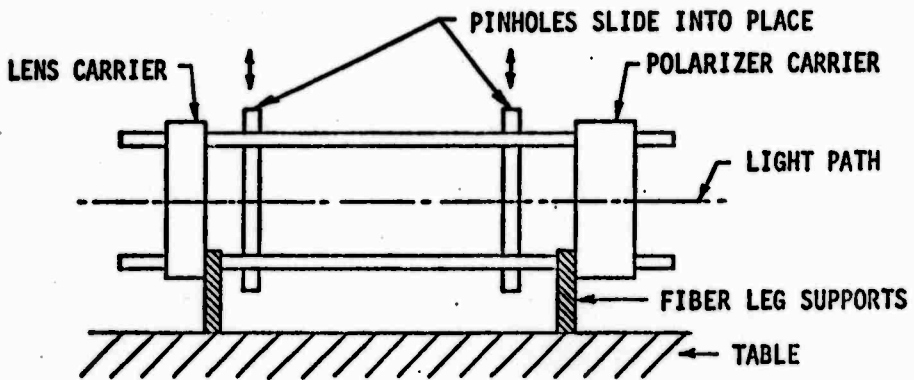


FIG. A.1--Indirect, far wall, spatial filter, alignment technique.



(a)



(b)

FIG. A.2--(a) 20 mil pinhole.
 (b) 2, 20 mil pinholes slide into place in a fiber leg to define a light path through the fiber leg.

(5) Remove the two 20 mil pinholes in the CCL fiber leg.

At this point the alignment beam is centered in the CL and CCL fiber legs.

(6) Adjust the acousto-optic modulator to get maximum power in the first diffraction order.

(7) Adjust the spatial filter to get maximum power throughput. Spatial beam should be properly filtered (i.e., single mode) and should be properly recollimated.

(8) Adjust mirrors M1 and M2 to cause the CCL input spatial beam to overlap the alignment spatial beam in two widely separated parallel planes. (Far wall alignment technique.)

At this point the CCL input spatial beam is coaxial and parallel with the alignment spatial beam.

(9) Block the input spatial beam anywhere before the spatial filter with an opaque screen.

(10) Adjust the beam splitter, BS, to cause the alignment beam to propagate backwards through the spatial filter. (Spatial filter alignment technique.)

(11) Unblock the input spatial beam and block the alignment spatial beam anywhere before the CL fiber leg.

(12) Insert two 20 mil pinholes in the CL fiber leg.

(13) If the CL input spatial beam does not pass through the pinholes (i.e., the input spatial beam is parallel to the alignment spatial beam but is displaced to the left or right of the alignment spatial beam), translate the beam splitter to achieve passage of the CL input spatial beam through the pinholes.

- (14) Repeat steps 9 through 13 until the alignment spatial beam propagates backward through the spatial filter and the CL input spatial beam propagates through two 20 mil pinholes in the CL fiber leg.

At this point the CL input spatial beam is coaxial and parallel to the alignment spatial beam. Tilting the beam splitter perturbs the alignment in the CCL leg in second order but this perturbation may be large enough to cause problems at times.

- (15) Check overlap of CCL spatial input beam and alignment spatial beam in two widely separated parallel planes. If a misalignment exists repeat steps 8 through 15 again.

At this point both the CCL and CL input spatial beams are coaxial and parallel to the alignment beam to tolerances which are given in Appendix F.

- (16) Remove the alignment laser and associated mirrors AM1 and AM2.
Install the coupling lenses in the CL and CCL fiber leg lens carriers.
- (17) Position and secure the fiber end positioners to the optics table at the ends of the fiber legs.
- (18) Adjust the fiber end position to obtain maximum coupling of the CCL and CL input spatial beams into the CCL and CL fiber ends respectively.
- (19) Adjust mirror M4 to steer output beam into detector aperture. Iris detector aperture.

System is now ready for operation. Operate acousto-optic modulator in pulsed mode. Turn on detector. Monitor detector output on scope. To achieve more recirculations at a reduced rotation sensitivity the following can be done.

- (20) By only using the z position adjustment of the CL fiber end positioner, translate the CL fiber end close to its coupling lens while monitoring the number of recirculations on the scope. When a maximum number of recirculations is obtained, stop.

At this point the system is optimized for recirculation but the coupling of the CL input spatial beam to the CL fiber end is perturbed. The perturbation results from translations in x and y of the fiber end which result from the z translation of the fiber end and from the z translation of the fiber end directly. It is possible to overcome the first perturbation by the following procedure.

- (21) Adjust the beam splitter, BS, to achieve a maxima for the coupling of the CL input spatial beam into the CL fiber end.

It is not possible to correct the perturbation in the coupling due directly to the z translation of the fiber end with this setup.

APPENDIX B

INDIRECT, DOUBLE FAR WALL ALIGNMENT TECHNIQUE

In this alignment technique, two counterpropagating alignment spatial beams are used. The two alignment spatial beams are first made to overlap. Then each input spatial beam is aligned to the alignment spatial beam which propagates in the same direction using the far wall alignment technique. This technique is indirect because the alignment for recirculation is achieved in an indirect manner by aligning the input spatial beams to their alignment spatial beams and then placing the fiber ends in such positions that the input spatial beams are coupled strongly into the fiber. At no point during the alignment procedure is the recirculation efficiency directly measurable.

In Fig. B-1, the layout of the optical components and spatial beams are shown.

The following set of instructions are the steps which were used in the laboratory for implementing this alignment technique.

- (1) Setup alignment laser, alignment beam splitter (ABS), and alignment beam steering mirrors AM1, AM2, AM3.
- (2) Install two 20 mil pinholes in the CL and CCL fiber loop.
- (3) Use ABS and AM1 to steer the CL alignment spatial beam through the two 20 mil pinholes in the CCL fiber leg.
- (4) Use AM2 and AM3 to steer the CCL alignment spatial beam through the two 20 mil pinholes in the CL fiber leg.
- (5) Remove the two 20 mil pinholes in the CCL fiber leg.
- (6) Block the CCL alignment beam just after ABS.
- (7) Adjust the prism directional coupler to send the CL alignment beam through the two 20 mil pinholes in the CL fiber leg.

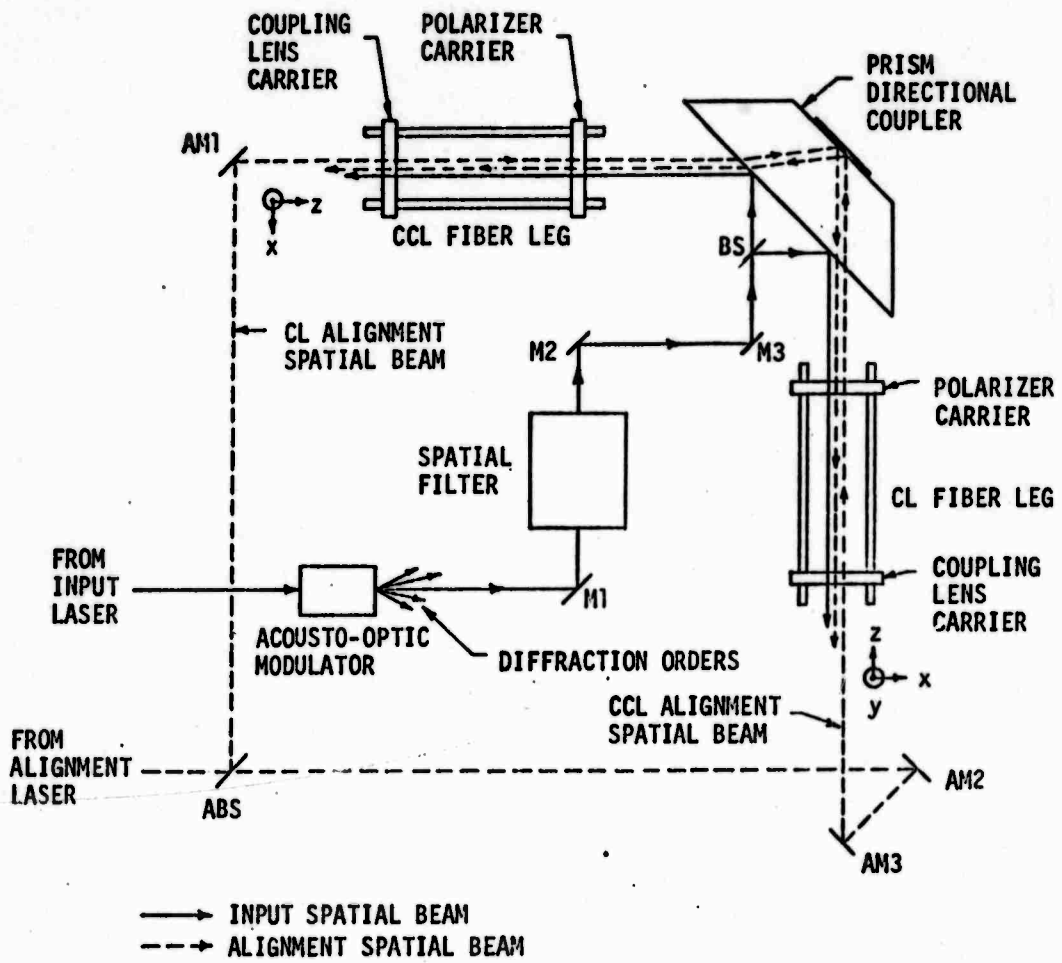


FIG. B.1--Indirect, double far wall alignment technique.

(8) Remove the 20 mil pinholes in the CL fiber leg.

At this point the counterpropagating alignment spatial beams are coaxial and parallel and they are centered in the fiber legs.

(9) Adjust the acousto-optic modulator for maximum power in the first diffraction order.

(10) Adjust mirror M1 and spatial filter to propagate the first diffraction order through the spatial filter with proper filtering (i.e., single mode) and with proper recollimation.

(11) Adjust mirrors M2 and M3 to cause the CCL input spatial beam to overlap the CCL alignment spatial beam in two widely separated, parallel planes.

(12) Adjust the beam splitter BS to cause the CL input spatial beam to overlap the CL alignment spatial beam in two widely separated, parallel planes.

(13) Check the overlap of the CCL input and alignment spatial beams to see if they have been perturbed. If they have been perturbed repeat steps 11 through 13 again.

At this point the input spatial beams are aligned to the recirculating path as defined by the alignment spatial beams.

(14) Remove the alignment laser and alignment optics.

(15) Install the coupling lenses in the CL and CCL lens carrier.

(16) Position and secure the fiber end positioners at the ends of the fiber legs.

(17) Adjust the fiber ends using the fiber end positioners to achieve maximum coupling of the input spatial beams into their respective fiber ends.

- (18) Adjust mirror M4 to send the output spatial beam to the detector.
Iris the detector.

The system is now ready to run. Switch the acousto-optic modulator to the pulsed mode. Turn on the detector and monitor the detector output on the oscilloscope.

If more recirculations at a lower rotation sensitivity are required the following procedure can be followed.

- (19) While monitoring the scope, translate the CL fiber end in the z-direction (see Fig. B-1) closer to its coupling lens. When the maximum number of recirculations is observed stop the translation.
- (20) Adjust the beam splitter, BS, to achieve a maximum of coupling of the CL input spatial beam into the CL fiber end.

With these additional steps, recirculation is optimized but the coupling of the C1 input spatial beam into the C1 fiber end is perturbed. There is no method of correcting this perturbation in this system configuration and alignment technique.

APPENDIX C

DIRECT ALIGNMENT TECHNIQUE

As the name of this alignment technique implies, the recirculating efficiency is directly monitored during the alignment procedure. The alignment is accomplished by using a short section of optical fiber as a target in one of the fiber legs. The N-turn loop of fiber is used as a source for the recirculating spatial beam in the other fiber leg. By adjusting the source and target fiber ends while monitoring the power coupled into the target fiber, one can find the global maxima of the recirculation efficiency.

This alignment technique was never implemented in its entirety due to lack of appropriate optical components and lack of physical space in the fiber-optic gyroscope to place these components. We tried this alignment technique in a limited manner and found that it worked as expected. Once the bugs are worked out of the implementation of this alignment technique, it promises to be the best of the three alignment techniques tried to date.

We will first cover the limited implementation of this alignment technique and then the full implementation of the alignment technique.

The following are the steps which were used in the limited implementation of this alignment technique. See Fig. C-1.

- (1) Check to make sure the coupling lenses are installed in their carriers.
- (2) Install one end of the target fiber in the CL fiber end positioner.
- (3) Adjust acousto-optic modulator for maximum power in first diffraction order.

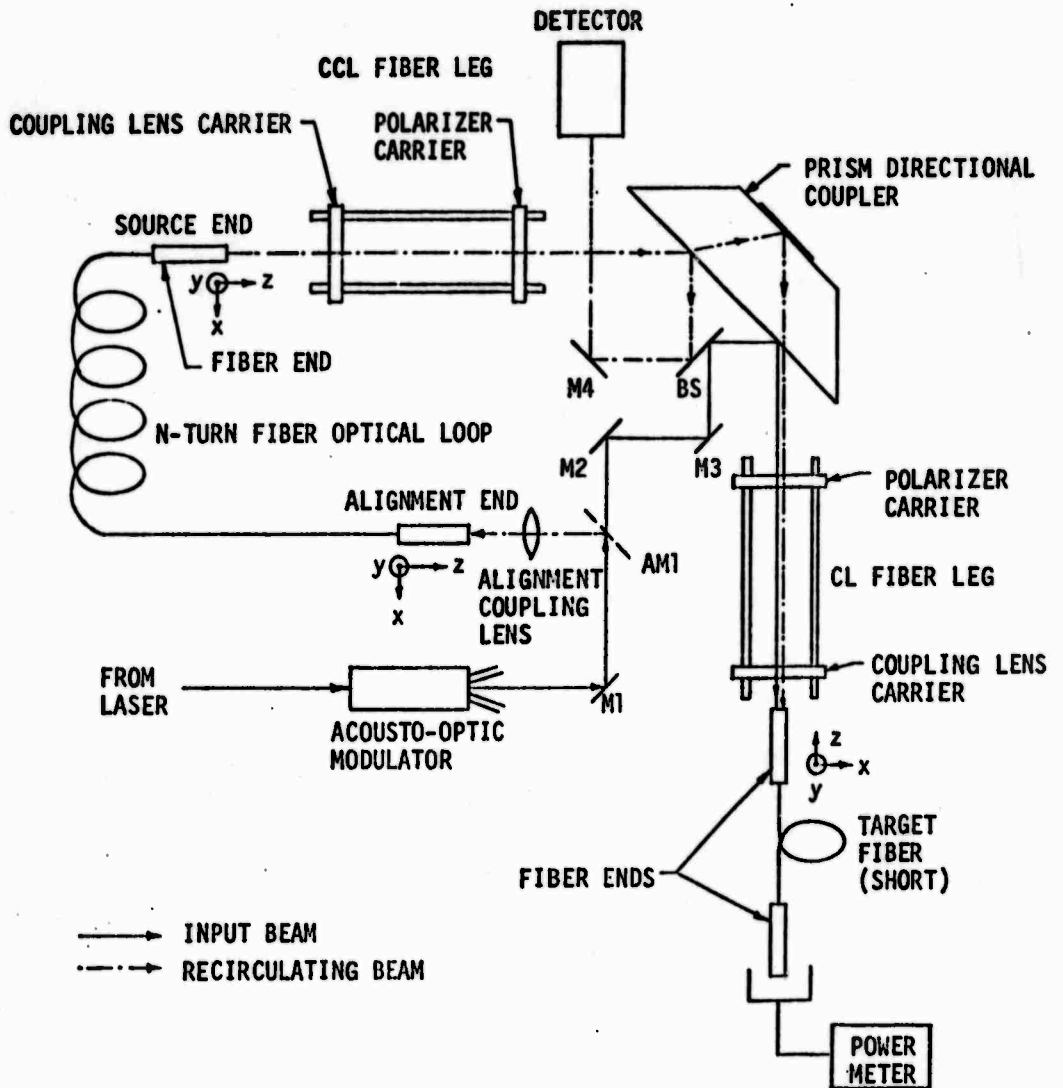


FIG. C.1--System configuration for limit implementation of direct alignment technique (fiber end positioners not shown).

- (4) Insert two 20 mil pinholes in the CL fiber leg.
- (5) Adjust mirrors M1, M2 and M3 and beam splitter, BS, to send the first diffraction order through the pinholes.
- (6) Remove the pinholes from the CL fiber leg.
- (7) Adjust the position of the target fiber end using the CL fiber end positioner for maximum input coupling.

At this point, the position of the target fiber end is marked in space by the waist of the focused Gaussian spatial beam. The accuracy to which this position is marked is $\pm 0.5 \mu\text{m}$ transversely and $\pm 10 \mu\text{m}$ longitudinally.

- (8) Install alignment mirror, AM1 to deflect the output of the acousto-optic modulator onto the alignment coupling lens without perturbing any of the previous settings.
- (9) Adjust the alignment end of the N-turn fiber optic loop so that the first diffraction order of the acousto-optic modulator is coupled into the alignment fiber end.
- (10) Adjust the source end of the N-turn fiber optic loop using the CCL fiber end positioner to achieve a maximum of coupling of the recirculating spatial beam into the target fiber.

At this point, the source end of the N-turn fiber optic loop is in the proper position for a local maxima of the recirculation efficiency.

- (11) Remove the target fiber from the CL fiber end positioner and insert the alignment end of the N-turn fiber optic loop into the CL fiber end positioner.

(12) Remove the alignment mirror A1.

(13) Adjust the CL fiber end positioner to optimize the input coupling of the CL input spatial beam into the CL end of the N-turn fiber optic (i.e., formerly was the alignment end).

At this point the CL end of the N-turn fiber optic loop is in the same spatial position as was the target fiber. The accuracies are $\pm 0.5 \mu\text{m}$ transversely and $\pm 10 \mu\text{m}$ longitudinally.

Now switch the acousto-optic modulator to the pulsed mode. Adjust mirror M4 to send the output in the detector. Iris the detector and observe the detector output on the scope.

This limited implementation of the alignment technique places us at a local maxima of the recirculating efficiency, hence we were only able to observe two echoes. See Appendix D for a discussion of recirculating efficiency.

For a full implementation of the direct alignment technique the system configuration is as shown in Fig. C-2. The only new components are the black boxes installed in the CL and CCL input legs. The black boxes consist of appropriate optical components and adjustments which allow us to vary independently of each other the radius of curvature and spot size of the input Gaussian beam at the coupling lens. Varying the radius of curvature of the Gaussian beam at the coupling lens is equivalent to translating the fiber end to or from the coupling lens as far as input coupling is concerned. Varying the spot size of the Gaussian beam at the coupling lens only changes the focused spot size to first order. With these black boxes we can couple the input beams into the fiber ends without having to move the fiber ends.

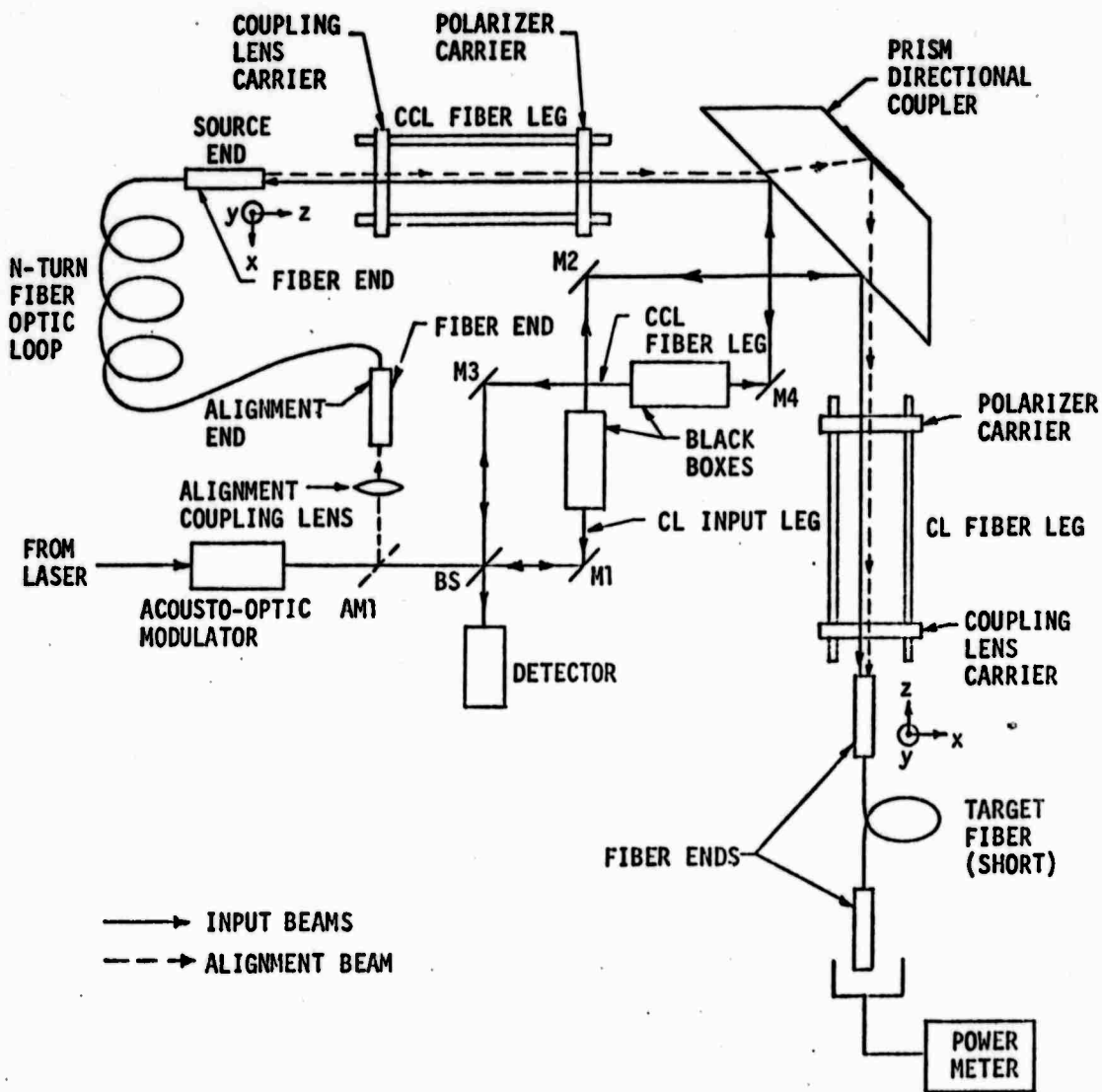


FIG. C.2--Proposed system configuration for full implementation of direct alignment technique.

The following set of instructions are what we propose to use to fully implement the direct alignment technique.

- (1) Install coupling lenses in their carriers.
- (2) Install one end of the target fiber in the CL fiber end positioner.
- (3) Install alignment mirror AM1 to deflect the output of acousto-optic modulator onto the alignment coupling lens. AO modulator can be off (i.e., no diffracted beams).
- (4) Adjust the alignment end of the N-turn fiber optic loop to achieve maximum input coupling.
- (5) Adjust the position of the source end of the N-turn fiber optic loop using the CCL fiber end positioner and the target fiber using the CL fiber end positioner while monitoring the throughput of the target fiber.
- (6) When the throughput is at a global maxima, stop. The system is now aligned for optimum recirculation efficiency.

We have actually performed this set of steps. Fig. C-3 shows the throughput loss of the light between the output of the AO modulator and the power meter at the end of the target fiber versus distance of the source end of the N-turn fiber optic loop to its coupling lens. The observed behavior is in accord with theory as described in Appendix D.

- (7) Remove the alignment mirror AM1.
- (8) Adjust the AO modulator for maximum power in the first diffraction order.

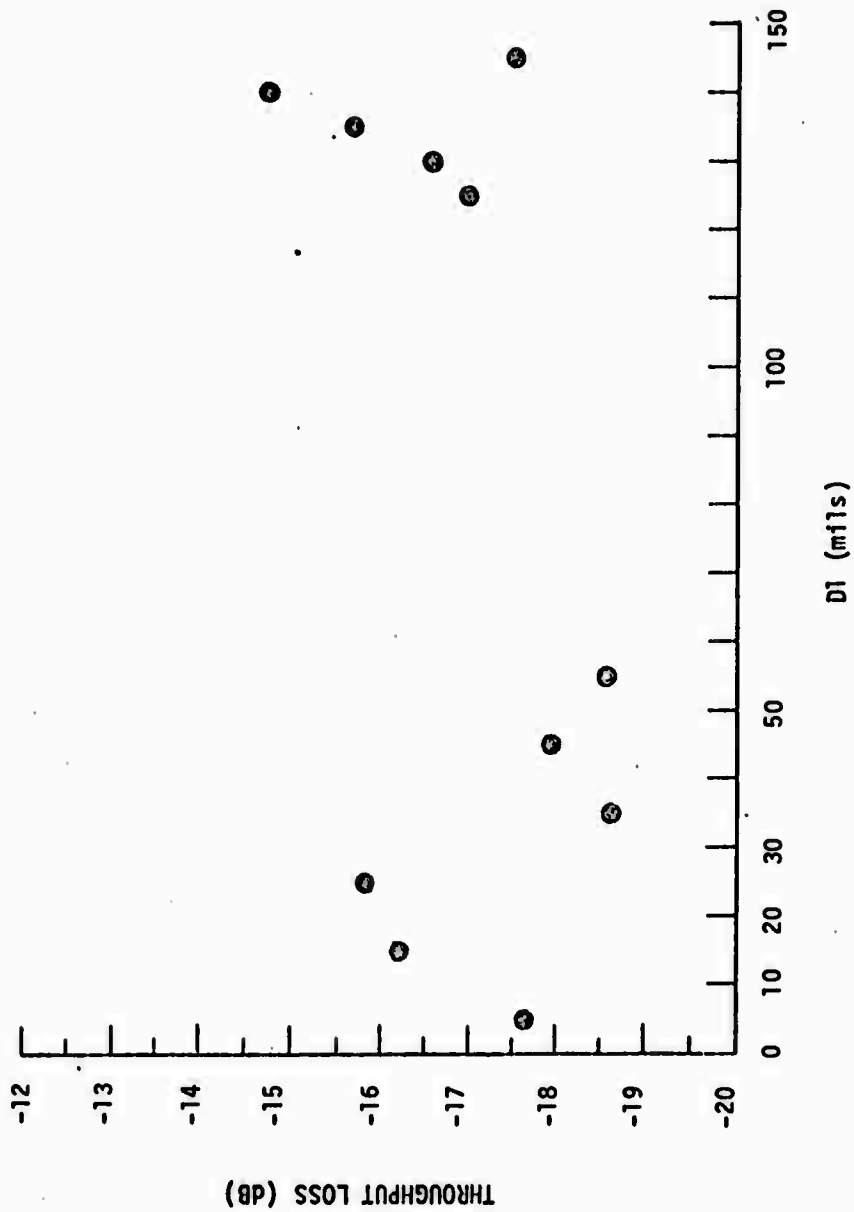


FIG. C.3--Throughput loss of recirculating beam vs. distance of source fiber end to coupling lens.

- (9) Using mirrors M1 and M2 and the black box in the CL input leg, arrange for maximum input coupling into the target fiber.

This marks the position of the target fiber end in space as described before.

- (10) Remove the target fiber from the CL fiber end positioner.
- (11) Install the alignment end of the N-turn fiber optic loop in the CL fiber end positioner.
- (12) Position the CL fiber end (formerly alignment end) using the CL fiber end positioner to achieve maximum input coupling from the CL input spatial beam.

The CL fiber end is now in the same position as was the target fiber end. The tolerances are the same as before.

- (13) Using mirrors M3 and M4 and the black box in the CCL input leg, arrange for maximum input coupling into the CCL fiber end (formerly source end).

The system is now aligned for maximum power inputs in both directions and for maximum recirculation.

- (14) Switch the AO modulator to pulsed operation.
- (15) Position and iris the detector.
- (16) Observe the detector output.

The required block boxes were never fabricated and hence this direct alignment technique was never fully implemented.

APPENDIX D

ALIGNMENT OF THE FIBER OPTIC GYROSCOPE FOR RECIRCULATION

In the fiber optic gyroscope, we have two input beams propagating in opposite directions and two recirculating beams also propagating in opposite directions. We have to align the spatial input beams to the spatial recirculating beams which propagate in the same direction.

The principle of reciprocity states that if one of the recirculating spatial beams couples into a fiber with some efficiency N_R then the other recirculating spatial beam will couple into the other fiber with the same efficiency N_R . The recirculating efficiency N_R is defined as the power coupled into one fiber divided by the power out of the other fiber. The principle of reciprocity assures us that once recirculation is achieved in one direction, it is achieved for both directions.

To efficiently couple the various spatial beams into the fiber we use coupling lenses. To achieve high efficiency in coupling into the fiber we want the overlap integral of the focused spatial beam and the fiber mode to be as large as possible. From maximizing the overlap integral, we determine that the fiber end should be located at the waist of the focused spatial beam and that the $1/e^2$ diameter of the spatial beam should match the core diameter of the fiber.

Hereafter, it will be assumed that two spatial beams are aligned with respect to coupling into one fiber end, if the power in the fiber due to one spatial beam is half that due to the other spatial beam.

The above criteria will put limits on the spatial positions of the focused waists of the spatial beams, on the waist size of the focused spatial beams, and on the angle between the focused spatial beams. The coupling lens will transform the above limits on the focused spatial beams into limits on the unfocused spatial beams. These limits are on co-axiality, parallelism, and complex radius of curvature of the unfocused spatial beams.

As derived in Appendix E the limits on the various parameters of the unfocused spatial beams are:

parallelism	0.11 mrad
co-axiality	0.7 mm
Δ (radius of curvature)	6.5 cm
Δ (waist size)	0.76 mm

In practice we can and have achieved the following limits of the above parameters:

parallelism	0.2 mrad ⁽¹⁾
co-axiality	0.5 mm ⁽¹⁾
Δ (radius of curvature)	125 cm ⁽²⁾ (with large laser)
Δ (waist size)	0.2 mm ⁽³⁾

Comparing actual with theoretical limits we see that we are within a factor of two on all limits except for the radius of curvature.

¹Obtained by using the "far-wall" alignment techniques. See Appendix F.

²Obtained from calculations based on the relative locations and sizes of the waists of the recirculating and input spatial beams.

³Directly measured at the coupling lens.

When using the small laser, the recirculating and input beams were close enough in complex radius of curvature, so that we regularly obtained two passes of the fiber optic loop. Both echoes were rotation sensitive. The power level of the laser was insufficient to provide a measurable third echo.

A diagram of the recirculating system is shown in Fig. 11. Shown are two fiber ends, two coupling lenses of focal length f separated by an interlens spacing L and the respective fiber end to coupling lens distances d_1 and d_2 .

The recirculating efficiency N_R (as defined on page 1) is a function of the spatial and angular positions of both fiber ends. If we neglect the angular and the transverse spatial dependence of N_R and think of N_R as a function of d_1 and d_2 only, we can make some powerful statements on the form of $N_R(d_1, d_2)$.

The recirculating efficiency $N_R(d_1, d_2)$ has two global maxima of equal value. These two global maxima correspond to spatial beam shapes between the fiber ends of the following form: the first spatial beam shape has a large waist ($\sim 2\text{mm}$) midway between the lenses, the second spatial beam shape has a small waist ($\sim 60\ \mu\text{m}$) midway between the lenses. For either of these spatial beam shapes the fiber-lens distances are equal. If d_2 say, is set to a different value than for either case above, d_1 can still be set to achieve a local maxima.

In aligning the system we proceed as follows. First we use one of the various alignment techniques to bring the recirculating and input beams into rough alignment, secondly we position both ends of the fiber at the focus of the input beams, thirdly we go into pulse operation and

observe the echoes on the oscilloscope and fourthly we adjust one fiber end while observing the echoes on the scope and trying to maximize their number and magnitude. The fourth step requires at least two echoes to be observable on the scope. If two echoes are not observed, we must start over again at step one (i.e., the rough alignment was not accurate enough).

For the above alignment procedure, let us assume that fiber end No. 1 is to be adjusted in step four for optimization of pulse number and magnitude. Fiber No. 2 was set at a position $d_{2,i}$ such that the input spatial beam was coupled into fiber end No. 2 with high efficiency. This value of $d_{2,i}$ is generally not the same as the value of d_2 which gives a maximum of the recirculating beam efficiency (N_R). As stated on the previous page d_1 can still be set to some value which provides a local maxima for N_R , but this value of d_1 is quite different from the value of $d_{1,i}$ (the position of fiber end No. 1 which provides for optimum input spatial beam coupling into fiber end No. 1).⁴ The recirculating beam efficiency (N_R) is the same for both directions, but we are only coupling input power into the fiber in one direction. The effect of this is that we have essentially power recirculating in one direction only. The pulses are now totally insensitive to rotation. We have observed this repeatedly. We have observed a maximum of five, rotation insensitive echoes.

How close do $d_{1,i}$ and $d_{2,i}$ have to be to d_1 and d_2 respectively to provide both effective coupling of input power into the fiber ends and recirculation? The answer is within one Rayleigh range of the focused spatial beam (for us this is 25 μm). To achieve this we must mode match the input spatial beams to the recirculating spatial beams. To accomplish this a lens or a set of lenses must be placed in the input spatial beam exterior to the loop.

⁴ measured $|d_{1,i} - d_1| = 0.5 \text{ mm}$.

APPENDIX E

BEAM PARAMETER TOLERANCES FOR SIMULTANEOUS COUPLING
OF TWO SPATIAL BEAMS INTO ONE OPTICAL FIBER

A Gaussian beam is assumed to have uniform power density over a circular area of radius w . The mode in a fiber is assumed to have uniform power density over a circular area of radius r_0 , where r_0 is the radius of the core. These approximations to the real modes allow easy evaluation of the overlap integral.

The overlap integral is

$$\frac{\int_A H_G H_F ds}{\left[\int_A H_G^2 ds \right]^{1/2} \left[\int_A H_F^2 ds \right]^{1/2}} = \text{coupling efficiency} \quad (1)$$

where H_G and H_F are the Gaussian and fiber modes and the integrations are carried out over the end of the fiber.

By varying the angle between two spatial beams before a lens, which focuses them into one fiber, the transverse spacing of the focused spots can be varied. When the centers of the spots are more than r_0 apart the overlap integral drops to less than 1/2 for one of the spatial beams (assuming the focused spot size w of each beam is equal to r_0 and one of the spatial beams has an overlap integral of 1).

The transverse displacement which is equal to r_0 in this case imposes a limit on the angle α between the spatial beams before the lens. From an ABCD matrix we get

$$\begin{aligned} (a) \quad r_0 &= f\alpha \\ (b) \quad \alpha &= r_0/f \end{aligned} \quad (2)$$

For the results given in Appendix D f was assumed to be 2 cm.

Using the ABCD matrix above we can get the angle β between the focused spatial beams as a function of the transverse displacement of the unfocused spatial beams.

$$\begin{aligned} \text{(a)} \quad \beta &= \Delta/f \\ \text{(b)} \quad \Delta &= f\beta \end{aligned} \tag{3}$$

We need to know for what value of β the overlap integral of (1) is equal to 1/2. An exact answer is difficult to obtain so an approximation is used. If a plane wave illuminates a surface at an angle, the phase shift (ϕ) across the surface is given as

$$\phi = kd \cos \theta \tag{4}$$

where k is the wavevector of the plane wave, θ is the angle between the surface and the wavevector, and d is the distance across the surface. Since the Gaussian beam is planar at a waist this is a good approximation. By substituting the phase shift across the surface (4) into the overlap integral (1), we can say that ϕ should vary by not more than $\pi/2$ across the core of the fiber. Hence θ or β is given as

$$\beta = \cos^{-1} \frac{\lambda}{8r_0} \tag{5}$$

Substituting (5) into (3b) we get the limit on the transverse displacement of unfocused spatial beams as

$$\Delta = f \cos^{-1} \frac{\lambda}{8r_0} \tag{6}$$

For the value of Δ given in Appendix D $f = 2 \text{ cm}$ and $\lambda = 6328 \text{ \AA}$.

The radius of curvature of a Gaussian beam determines the plane in space behind the lens in which the waist of the focused Gaussian beam will be. For $\pi w^2/\lambda \gg f$ (w evaluated at the lens) we can write for the distance d at which the waist is focused as

$$d = \frac{f}{1 - f/R} \quad (7)$$

From this we can write the difference in $(1/d)$ caused by a difference in $(1/R)$.

$$\Delta(1/d) = -\Delta(1/R) \quad (8)$$

if $\Delta(d)$ is small then $\Delta(1/d) \sim -\Delta d/d^2$ and if $d \approx f$ then we can write

$$(a) \quad \Delta d \approx f^2 \Delta(1/R) \quad (9)$$

$$(b) \quad \Delta R \approx R^2/f^2 \Delta d \quad (\Delta(R) \text{ small})$$

For what Δd is the overlap integral equal to $1/2$? If we remember that a Gaussian beam has twice the area at a distance of one Rayleigh range from the waist, as at the waist, we see that $\Delta d =$ one Rayleigh range which for us is $25 \mu\text{m}$.

Lastly, for what value of the difference in focused waist sizes, Δw is the overlap integral (1) equal to $1/2$? We want the area of one beam to be twice as large as the area of the other beam, hence we have:

$$\Delta w_f = (\sqrt{2} - 1) w \quad (10)$$

For the result given in Appendix D w is taken to be $2.25 \mu\text{m}$. The focused difference in waist size (Δw_f) can be related to the unfocused difference in spot (Δw) size as

$$\Delta w = f\lambda/\pi \Delta(1/w_f) \quad (11)$$

if $\Delta(w_f)$ small, then it is given by $-\Delta w_f/w_f^2$ and hence Δw is given by combining (10) and (11) as

$$\Delta w = (f\lambda/\pi w_f^2) \Delta w_f = (f\lambda/\pi w_f) (2 - 1) \quad (12)$$

For the results stated in Appendix D, $f = 2 \text{ cm}$, $\lambda = 6328 \text{ \AA}$, $w_f = 2.25 \mu\text{m}$.

Finally, it is important to note that a misalignment in each of the above four areas (coaxiality, parallelism, radius of curvature, and spot size) are not independent. It is possible to get a cumulative effect for misalignments. In some cases it is possible for misalignments in two or more areas to partially cancel each other.

APPENDIX F

ACCURACIES OF VARIOUS TECHNIQUES FOR SPATIAL AND ANGULAR ALIGNMENT OF TWO SPATIAL BEAMS

This appendix examines the accuracies which are achievable by various techniques of aligning two spatial beams. These techniques are the far-wall technique, the pin-hole technique and the spatial filter technique.

In analyzing each of these techniques geometric optics are used.

I. Far Wall Technique

The situation is shown in Fig. F-1. Two collimated beams of light have their centers closer together than some distance σ in two parallel planes which are separated by a distance d .

The two beams of light are co-axial within a distance σ simply.

The two beams of light are parallel within θ radians where θ is given approximately as

$$\theta = 2\sigma/d \quad (1)$$

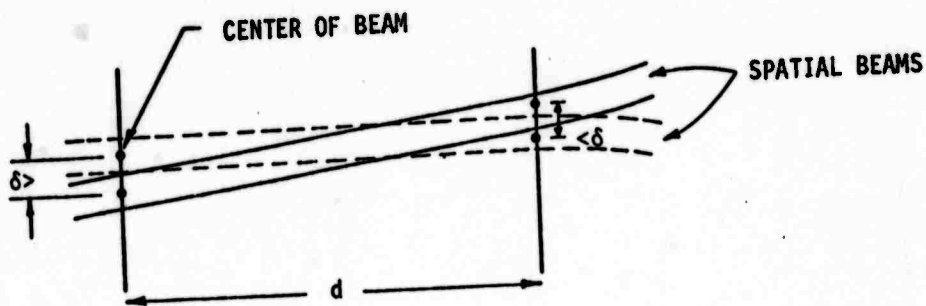
By using this technique we were able to achieve σ 's of about 0.5 mm and distances of 5 m. The accuracies of this technique were

$$\text{coaxiality} = 0.5 \text{ mm}$$

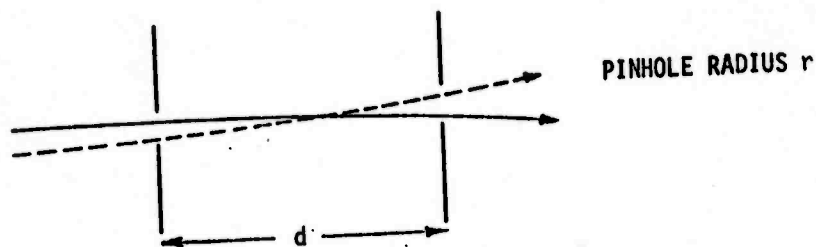
$$\text{parallelism} = 0.2 \text{ mrad}$$

II. Pinhole Alignment Technique

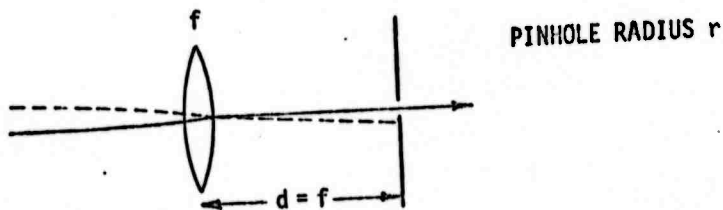
Figure F.2 shows two rays of light propagating through two pinholes of radius r separated by a distance d . This technique is identical to the farwall technique.



(F.1)



(F.2)



(F.3)

FIG. F.1--Far wall alignment of two collimated spatial beams.
 F.2--Pinhole alignment of two collimated spatial beams.
 F.3--Spatial filter alignment of two collimated spatial beams.

By observing a pinhole from behind we were able to detect displacements, , greater than $r/2$. Substitution this value in Eq. (1) we get the angular alignment accuracy

$$\theta = r/d \quad (2)$$

In using this technique, the pinhole diameters were 20 mils (0.5 mm) and the distance between pinholes was about 2 inches. The accuracies of this technique were

$$\begin{aligned} \text{coaxiality} &= 0.25 \text{ mm} \\ \text{parallelism} &= 10 \text{ mrad} \end{aligned}$$

III. Spatial Filter Technique

Figure F.3 shows the essential components for this alignment technique, namely a lens (or set of lens) with focal length f and a pinhole of radius r .

This technique is only for aligning two beams in angle. The lens brings all parallel light rays to the same point in the focal plane. Rays which are not parallel are brought to different points in the focal plane.

Using ABCD matrices we obtain the following relation for the transverse displacement σ of two rays in the focal plane of a lens.

$$\sigma = f\alpha \quad (3)$$

In Eq. (3), α is the angle between the two rays before the lens and f is the focal length of the lens.

Observing from behind the pinhole we can detect displacements σ between the two rays greater than $r/2$. Substituting this in Eq. (3) and solving for α we get

$$\alpha = \frac{r}{2f} \quad (4)$$

We frequently use a microscope objective instead of a lens. We approximate the focal length of a microscope objective as

$$f(\text{mm}) = \frac{165}{p} \quad (5)$$

where p is the power of the microscope objective.

Substituting Eq. (5) into Eq. (4) we get

$$\alpha = \frac{rp}{330} \quad (r \text{ expressed in mm}) \quad (6)$$

Either Eq. (4) or Eq. (6) can be used to calculate the angular accuracy of this alignment technique.

In using this technique the pinhole diameter was $5 \mu\text{m}$ and we used a 40x microscope objective. The angular accuracy of this technique was

parallelism: 0.6 mrad .

As stated in Appendix D the required accuracies of alignment are

parallelism: 0.11 mrad .

co-axiality: 0.7 mm .

We are able to meet the co-axiality requirement and almost meet the parallelism requirement.

APPENDIX G

HYBRID DIRECTIONAL COUPLERS FOR USE WITH A CLOSED FIBER OPTICAL LOOP

In our system a pulse of light propagates around a closed optical loop many times. After each transit of the loop it must be sampled. Further we have pulses propagating in each direction around the closed loop.

These facts lead to the following requirements for a hybrid directional coupler:

- (1) The coupler must close the optical loop.
- (2) It must provide for input and output coupling to and from the loop.
- (3) It must be bi-directional. It must couple into or out of the optical loop in both directions simultaneously.

With these requirements in mind we first designed and built the prism directional coupler shown in Fig. G.1. The coupler consists of a piece of optical glass whose front and rear surfaces are flat and parallel. The rear surface of the coupler is coated with gold to act as a mirror. This rear surface closes the optical loop. First surface reflections from the front surface of the coupler provides coupling into and out of the closed optical loop.

In Fig. G.1 the details of the operation of the prism directional coupler are shown. Also shown are the fiber ends, coupling lenses, central beam splitter, and beam steering mirrors.

The problem with the prism directional coupler was that the recirculating spatial beam could not be adjusted independently of the input spatial beam. This meant that once some recirculation was observed, the recirculation could not be tuned up without perturbing the input power significantly. With reduced input power, no recirculation is observable.

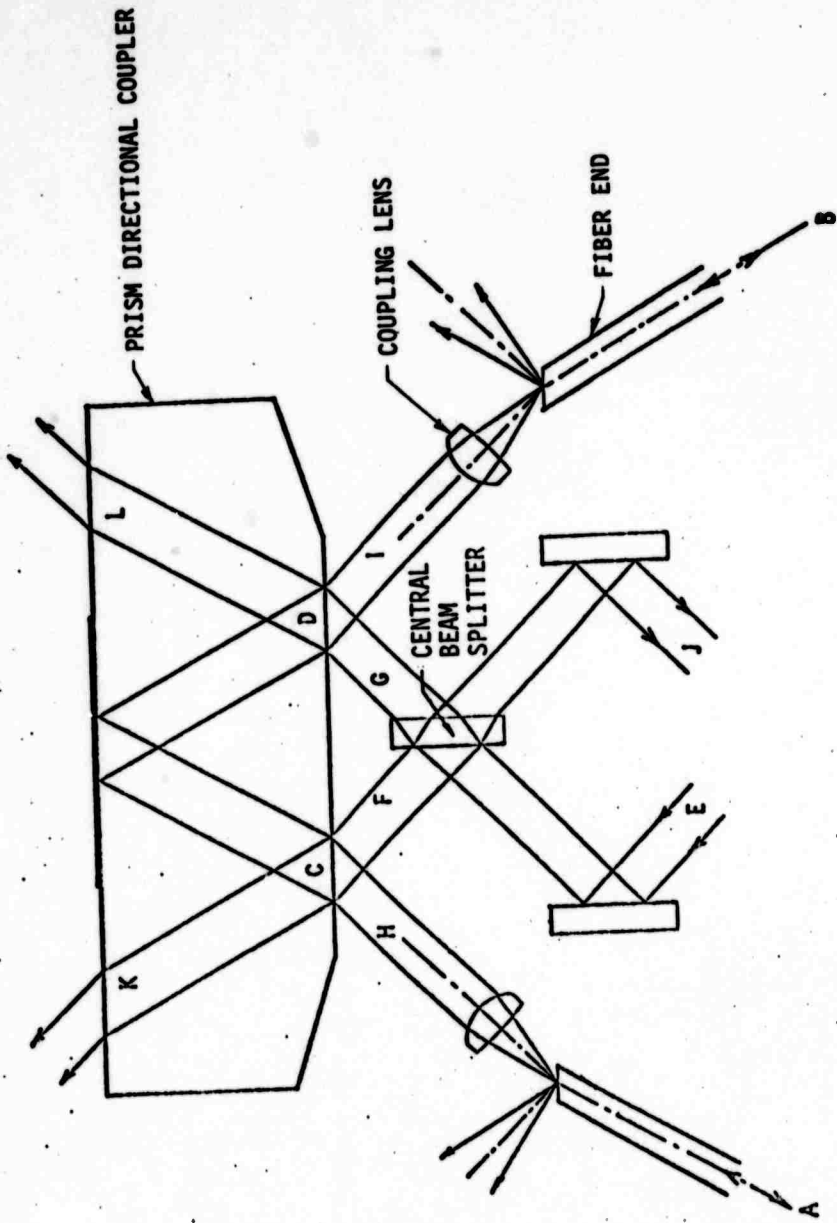


FIG. G.1--Prism directional coupler details.

To overcome this problem we temporarily replaced the prism directional coupler with two optical blanks and two first surface mirrors. Figure G.2 shows the details of this bidirectional coupler.

Comparing Figs. G.1 and G.2 one sees that the optical blanks act as the front surface of the prism directional coupler, and the recirculating mirrors act as the rear surface of the prism directional coupler.

By adjusting the recirculation mirrors one can control the recirculating spatial beams without perturbing the input spatial beams. Furthermore, placing a lens or a combination of lenses between the recirculation mirrors allows one to control the spatial profile of the recirculating spatial beam without perturbing the input spatial beam. This is important for modematching the input and recirculating spatial beams. By adjusting the optical blanks one controls the input spatial beams directly and causes a small transverse displacement of the recirculating spatial beam.

This system has a higher throughput loss due to first surface reflection at both front and back faces of the optical blanks and to higher scattering losses from the recirculation mirrors. The measured power loss¹ of this system is 3 dB while the prism directional coupler is only 1.8 dB. By AR coating one side of the optical blanks and using better quality recirculation mirrors we could lower the loss to that of the prism directional coupler.

This system did not work satisfactorily because the positioners for the optical blanks and the recirculation mirrors were of poor quality. They were not very stable and their adjustments were too coarse.

¹Power loss is measured between points H and I in Figs. 1 and 2.

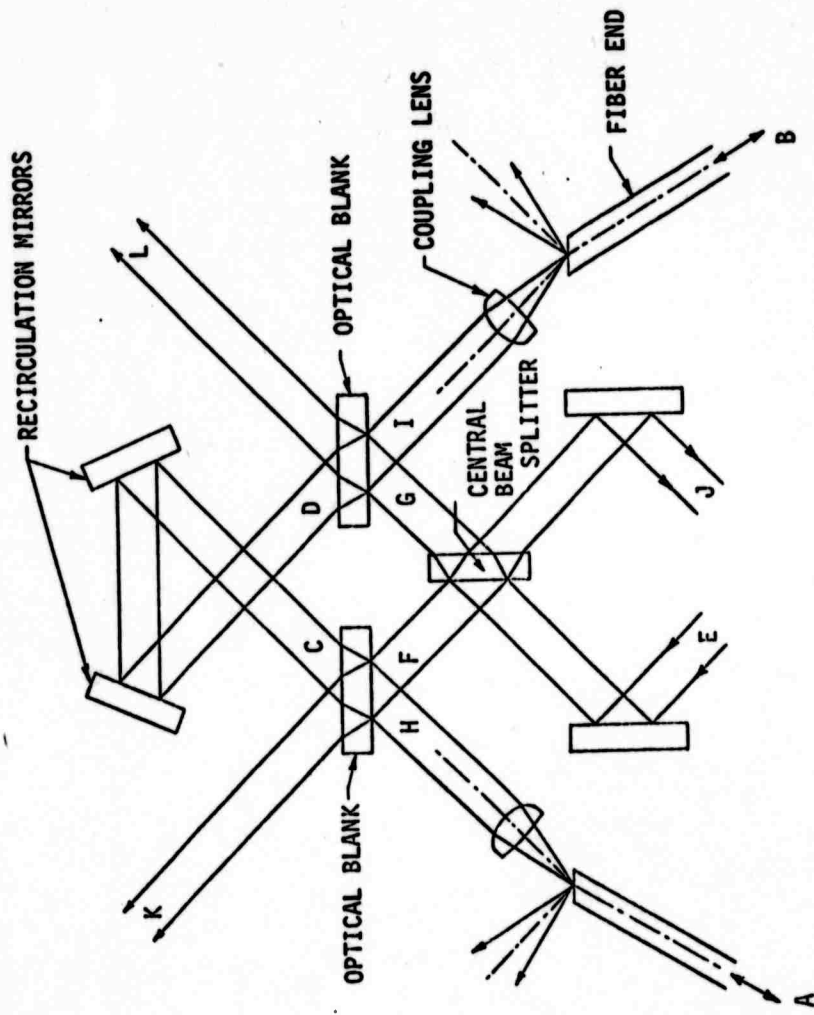


FIG. 6.2--Bidirectional coupler details.

With better quality positioners we feel that this system can be made to function properly.

Our development of a single mode fiber-to-fiber four port directional coupler has rendered further work on hybrid directional couplers unnecessary.